

**Diagnostic Analysis of Tropical
Cumulonimbus Downdraft Structure**

By

Maria Faus Silva Dias

Department of Atmospheric Science
Colorado State University
Fort Collins, Colorado



**Department of
Atmospheric Science**

Paper No. 272

DIAGNOSTIC ANALYSIS OF TROPICAL CUMULONIMBUS
DOWNDRAFT STRUCTURE

by

Maria Faus Silva Dias

Research Report supported by
The Global Atmospheric Research Program,
National Science Foundation and the
GATE Project Office, NOAA under grant
OCD 74-21678.

Principal Investigators: A.K. Betts and S.K. Cox

Department of Atmospheric Science
Colorado State University
Fort Collins, Colorado

June 1977.

Atmospheric Science Paper No. 272.

ACKNOWLEDGEMENTS

I would like to thank Dr. Alan K. Betts for his guidance and encouragement throughout this work. I also benefitted from discussions with Drs. William Cotton, David Krueger and Mr. Pedro Silva Dias.

This research was done while on leave from the Departamento de Meteorologia of the Instituto Astronômico e Geofísico of the Universidade de São Paulo, Brazil. The Conselho Nacional de Desenvolvimento Científico e Tecnológico-CNPq provided the scholarship.

Many thanks go to Ms. P. Martin who revised the text, Ms. S. Wunch who typed the manuscript and to Ms. Janella Owen who drafted the figures.

This research was supported by the Global Atmospheric Research Program National Science Foundation; and the GATE Project Office NOAA under Grant QCD-74-21678.

TABLE OF CONTENTS

	<u>PAGE</u>
ABSTRACT	ii
ACKNOWLEDGEMENTS	iii
TABLE OF CONTENTS	iv
LIST OF TABLES	vi
LIST OF FIGURES	vii
I. INTRODUCTION	1
II. REVIEW OF PAST AND RECENT WORK CONCERNING THE DOWNDRAFT IN CUMULI	2
2.1 Initiation and maintenance of the downdraft.	2
2.2 Some results from numerical simulations.	11
2.3 Conclusion.	17
III. THE EVAPORATION IN THE DOWNDRAFT CURRENT	18
3.1 Governing equations	19
3.1.1 Single drop case.	19
3.1.2 Drop spectrum case	23
3.1.3 Equations with a constant divergence profile.	33
3.1.4 Parameterization of the evaporation equation.	36
3.2 Initial conditions of temperature and moisture	38
3.2.1 Conditions corresponding to Betts (1976) model.	39
3.2.2 Conditions for a constant θ_E sounding.	41
3.3 Required rainfall intensities, downdraft speeds and drop spectrum.	44
3.3.1 Results for the mean "before" and "after" conditions (Model Figure 3.3).	44
3.3.2 Results for all soundings.	51

TABLE OF CONTENTS (Continued)

	<u>PAGE</u>
3.3.3 Results for constant θ_E soundings.	54
3.3.4 Comparison with data.	62
3.4 Vertical variation of some calculated variables	69
3.4.1 Profile of potential temperature.	70
3.4.2 Depletion of rainfall intensities and drop radius.	70
IV. MODELLING CONCLUSIONS	73
4.1 The parameter π_E vs. pre-storm parameters.	73
4.2 Analytical solution of the evaporation equation.	76
4.3 Suggestions for future research	79
V. SUMMARY AND CONCLUSIONS	84
REFERENCES	86

LIST OF TABLES

<u>TABLE</u>		<u>PAGE</u>
1	Variation of λ as a function of rainfall intensity and type of rain as specified by the parameters b and β .	27
2	Ventilation coefficient as a function of drop radius as given by Eq. 3.33, by Frossling (1938) and Kinzer and Gunn (1951).	30
3	Initial and final layer averaged conditions for the mean soundings and for 24 pairs of before - after soundings. For a given system there is only one before sounding but there may be one, two or three after soundings.	42
4	Initial conditions for the soundings which had a reasonably deep layer of constant θ_E . The conditions shown refer to the top of the constant θ_E layer.	45
5	Variation of the parameters $\pi_E(p_I)$ and α in the constant mass flux case for different values of drop radii, downdraft speeds and rainfall intensities.	52
6	Same as Table 5, for the constant divergence case .	53
7	Parameters $\pi_E(p_I)$ and α for all soundings.	55
8	Total rainfall and maximum rainfall intensity at seven stations located within 20 km from Carrizal in the time intervals between soundings.	61
9	Comparison of the downdraft speed as calculated using the parameters of Table 7 with the maximum observed deviation of the rawinsonde from a constant rate of ascent.	63
10	Ratio between rainfall intensities, drop radius or drop distribution parameters at the top and at the bottom of the layer for different initial conditions.	65

LIST OF FIGURES

<u>FIGURE</u>	<u>PAGE</u>
1.1 From Betts (1976).	7
2.1 From Kamburova and Ludlam (1966).	9
3.1 Computational scheme for the single drop approach.	24
3.2 Computational scheme for the drop spectrum approach.	32
3.3 Downdraft trajectory according to Betts (1976) model.	40
3.4 Potential temperature and equivalent potential temperature for the mean "before" and "after" soundings.	43
3.5 Initial rainfall intensities and downdraft speeds for different drop distributions.	46
3.6 Initial rainfall intensities and downdraft speeds for different drop distributions using as reference the "thunderstorm" curve of Fig. 3.5.	48
3.7 Variation of $\Delta\chi$ and π_E for the constant mass flux case.	49
3.8 Same as Fig. 3.7 for the constant divergence case.	50
3.9 Potential temperature and equivalent potential temperature in sounding 82 and as calculated using the constant mass flux approach.	56
3.10 Same as Fig. 3.9, for sounding 317.	57
3.11 Same as Fig. 3.10, for sounding 325. The profile of potential temperature from the constant divergence approach is also shown.	58
3.12 Deviation of the rawinsonde from a constant rate of ascent during sounding 325 and profile of vertical velocity imposed on the constant divergence approach.	59
3.13 Locations of recording rain gauges. WG4 is located at Carrizal, Venezuela (9° 22.8'N, 66° 55.0'W).	64
3.14 Vertical profile of potential temperature obtained using the constant mass flux and constant divergence approaches, using the mean "before" and "after" conditions.	66

LIST OF FIGURES (Continued)

<u>FIGURE</u>		<u>PAGE</u>
3.15	Vertical profile of mixing ratio obtained using the constant mass flux and constant divergence approaches, using the mean "before" and "after" conditions.	67
3.16	Drop spectrum variation with height for the Manton and Cotton (1977) and Kessler (1969) parameterizations.	68
4.1	A plot of $\pi_E(p_I)^{-1}$ vs. lower layer averaged relative humidity for the constant mass flux and constant divergence approaches.	72
4.2	A plot of $\pi_E(p_I)^{-1}$ vs. upper layer averaged relative humidity (b,e), depth of the subcloud layer (a,d) and relative inflow of air into the storm (c,f).	75
4.3	The variation of mixing ratio along a constant θ_E line $d\chi'/dp$ may be approximated, according to the above diagram, by $\Delta\chi/p$.	78
4.4	Vertical profiles of potential temperature, mixing ratio and relative humidity for different values of π_E (constant mass flux approach) for different starting conditions.	80
4.5	A plot of π_E against the mean value of p for the subcloud layer after the storm passage. The dashed line indicates the condition $\pi_E = P$.	81

I. INTRODUCTION

The downdraft circulation in cumulonimbus clouds has been receiving increasing attention due to its importance in the modelling and simulation of severe storms, squall lines and their relation to large scale motions. Many observational facts are known about the kind of circulation involved in cumulonimbus clouds but there are still more things to be understood. Ludlam (1963) developed a physical picture of the idealized updraft-downdraft circulation in a cumulonimbus cloud. The picture has evolved since then, and may be seen in two dimensions in the work of Betts (1976) reproduced here in Fig. 1.1 This figure shows a tropical cumulonimbus cloud with inflow in the front and outflow in upper levels in the rear. Since the observations of the Thunderstorm Project (1948) it has been known that the downdraft usually appears with the beginning of rain at the ground. The difference in the structure of the updraft and the downdraft is mainly that the former occurs under saturated conditions while the latter is subsaturated. If the forced up-current reaches the lifting condensation level, water vapor starts to condense in it and the release of latent heat accelerates the current upwards. The updraft will be under saturated conditions and droplets will be growing in it. Several theories have been presented in order to account for the initiation of the downdraft, but once started it can be maintained by the evaporation of raindrops which will cool the air which will descend and form a "cold pool". The evaporation in the downdraft is not sufficient to keep it saturated even under falling rain primarily because the compressional warming in the descending air allows for a higher moisture content than the one provided by evaporation of

raindrops. As shown by Kamburova and Ludlam (1966), the degree of sub-saturation will depend on the intensity of rain, the speed of the downdraft current and the size of raindrops.

The purpose of this research is to study the effect of the downdraft on the subcloud layer by determining the variability of the parameters which determine its structure and to isolate the parameters that are suitable for modelling the effect of the downdraft on the large scale. In Chapter 2, a review of past and recent studies is presented; in Chapter 3, a simple set of equations for a one dimensional flow governing the evaporation in a downdraft current is derived and discussed, the results from it presented and the variability of the involved parameters analyzed. This simple set of equations is modified in order to allow a realistic profile of the downdraft speed and the results are also presented and discussed. Chapter 4 discusses the implications of some results of Chapter 3 in terms of modelling. Chapter 5 presents the summary and conclusions.

II. REVIEW OF PAST AND RECENT WORK CONCERNING THE DOWNDRAFT IN CUMULI

The importance of the role that downdrafts play in the mature and dissipating stages of a thunderstorm was first recognized by Byers and Braham (1949). They observed that with the beginning of rain at the ground a downdraft appeared in the cloud; the downdraft remained unsaturated even in the presence of large amounts of precipitation and did not warm at an adiabatic lapse-rate but was cooler than the environment at the same level. At the ground, the downdraft air spreads predominantly to one side of the cell, behind a well marked micro-cold front, where its speed was a maximum. New cells formed above this outflow.

In the next sections of this chapter we summarize the research that has been directed towards explaining and modelling the structure of the downdraft air since the publication of the experimental results of the Thunderstorm Project.

2.1 Initiation and maintenance of the downdraft

The apparent anomaly of the unsaturated downdraft might be due, according to Byers and Braham (1949), to one of the two following processes. Firstly the downdraft may be dried out by cold precipitating particles. If the rain or hail is sufficiently colder than the ambient air, the water vapor pressure near the surface of these particles will be lower than that of the surroundings, resulting in a water vapor flux directed towards the particles which will grow and so reduce the ambient air water vapor. The second process suggested was that the downdraft is unable to remain saturated because the rate of evaporation of raindrops is too slow to provide for the increase in the saturation mixing ratio as the air descends to lower levels. In that case, the downdraft

air could be heated at a lapse-rate between the dry and the moist adiabatic processes and would reach the ground in an unsaturated state.

A process for the initiation of downdrafts was suggested by Squires (1958) based on the evidence that the average lapse-rate inside cumuli is steeper than the moist adiabatic one and that the ratio between the liquid water content to its adiabatic value (Q/Q_A) decreases rapidly with height. He elaborated a theory in which the downdraft would be initiated by entrainment of dry air: a parcel of dry air which entered the top of a growing cloud by turbulent diffusion would be cooled by evaporation of liquid water and might subside into the cloud, thus explaining why Q/Q_A decreases with height. The initiation could also take place due to the drag of falling raindrops as pointed out by Das (1964) who simulated this process for the first time in a numerical model. He neglected the effects of entrainment of dry air as an initiator of the downdraft. This model does not include an interaction between the cloud and the environmental atmosphere such as entrainment, the effect of which is important in the life cycle of a convective cloud.

Ludlam (1963) considered the airflow in hailstorms and how it depends upon the wind shear. He pointed out that when there is little or no wind shear the updraft is vertical and the precipitation falls through and impedes it. A pronounced downdraft can be produced only if the convection is intermittent so that the updraft consists of a succession of thermals from which precipitation can fall. The downdrafts spread out predominantly on one side when the ground has some slope, or in the presence of some shear. When there is a stronger wind shear the updraft becomes tilted and the outflow in the anvil aloft occurs predominantly on one side. This arrangement, according to Ludlam (1963)

offers the possibility of having the updraft and downdraft working continuously side by side.

Zipser (1969) using some data from the Line Islands Experiment suggested that the air which takes place in the downdraft circulations comes from the middle troposphere where the equivalent potential temperature (θ_E) is of the order of 330°K. He observed the complete absence of convective clouds throughout most of the downdraft area and concluded that in spite of its large magnitude, the addition of heat and moisture to the air below it was insufficient to restore cumulus development for 6-12 hours. This air was, therefore, completely unable to take part in the deep convection required to maintain tropical disturbances and, in fact, killed such convection everywhere that it spread. He suggested two processes by which the volume of the downdraft could be increased in the lower troposphere: first, this air could flow freely under the heavily raining anvil on a large-scale and sink in a direct circulation to the lower troposphere while remaining highly unsaturated. Second, it could be entrained directly into individual convective towers, also forming unsaturated downdrafts immediately downshear of the towers on a convective scale or mesoscale.

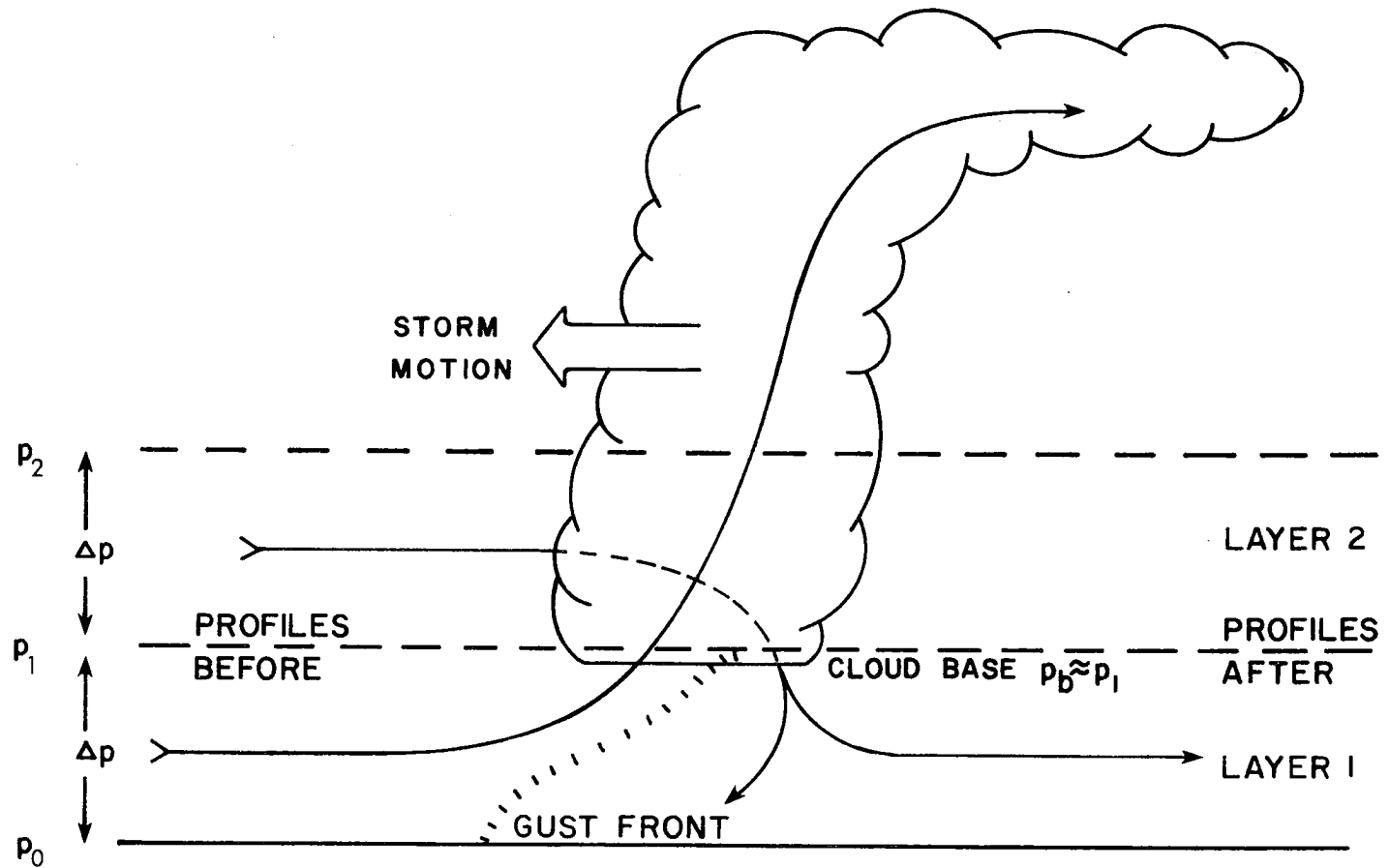
The structure of the downdraft as described by Zipser (1969) was confirmed in the work of Ruiz (1975) who used VIMHEX-1972 data (Venezuelan International Meteorological and Hydrological Experiment), although he pointed out that whether the sinking occurred in convective scale downdrafts or by large scale sinking under raining middle cloud decks, or both, was questionable.

Also using the VIMHEX-1972 data, Betts (1976) developed a simple model in order to explain the sub cloud layer structure after the

passage of a raining system (see Fig. 1.1 for a sketch of the model). In a typical case the preceding sounding showed an undisturbed atmospheric structure with a well defined nearly mixed layer up to cloud base while after the passage of a system the sounding showed a very different atmospheric structure with a cooling of the lower layer and a fall of equivalent potential temperature. Since the evaporation of falling rain into the sub cloud layer would produce a cooling and stabilization at constant θ_E , only a mass transport from upper layers could produce the observed fall of θ_E . He concluded that the air in the downdraft gust came from just above cloud base. Even in the deeper cases the downdraft air came mainly from below 700 mb which represents a shallower downdraft than the one found by Zipser (1969). Betts (1973), in a composite cumulonimbus study, found that in the mean system downdrafts did not extend from the mid-troposphere to near the surface, but air typically was descending 80 mb in downdrafts.

In two case studies Seguin and Garstang (1976) examined the coupling of cloud and sub cloud layers by precipitation downdrafts during disturbed and undisturbed conditions. They attribute the subsiding motion to the evaporation of cloud material and precipitation around the edges of the cloud line and conclude that these downdrafts must serve to balance the vertical transport of mass which takes place inside the active growing cloud in accordance with Gray's (1973) ideas.

The theories about the maintenance of the downdrafts are mostly based on the evaporation and drag force of falling raindrops. The temperature at the surface of evaporating raindrops was proved to be given, with good approximation, by the wet bulb temperature. This was shown empirically by Kinzer and Gunn (1951) and mathematically by Syono and



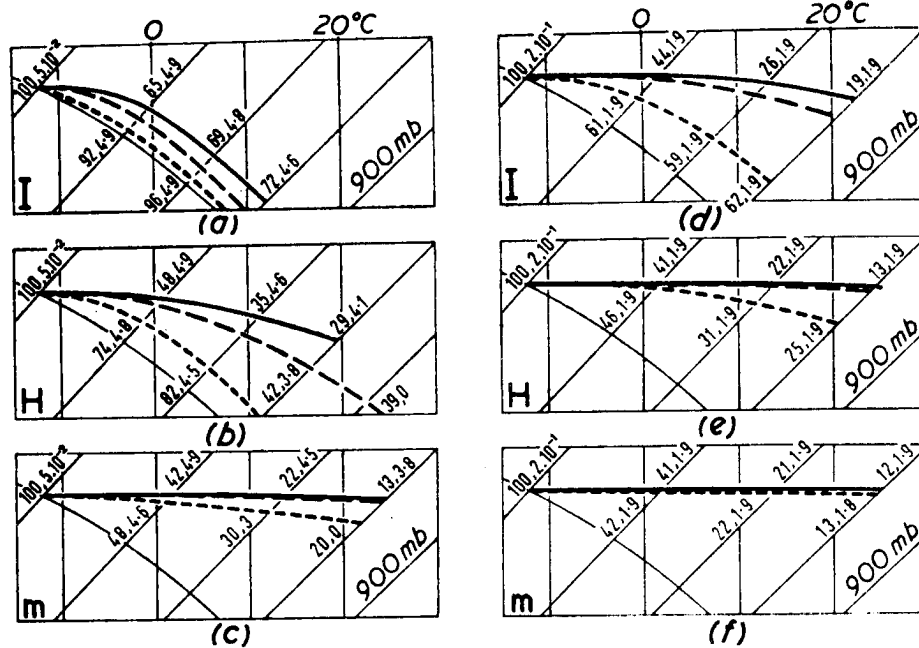
1. Schematic airflow relative to travelling mesosystem, showing two layer model exchange: inflow layer p_0 to p_1 ascends in updrafts and inflow layer p_1 to p_2 descends in downdrafts in replacement. (Actual flow inside system will be both three dimensional and transient, not two dimensional as sketched.)

Figure 1.1 From Betts (1976).

Takeda (1962), who also showed that the size-spectrum of raindrops changes with time due to evaporation and that, in comparison with large raindrops, the evaporation of small raindrops gives a considerably larger effect on the change of the atmospheric state.

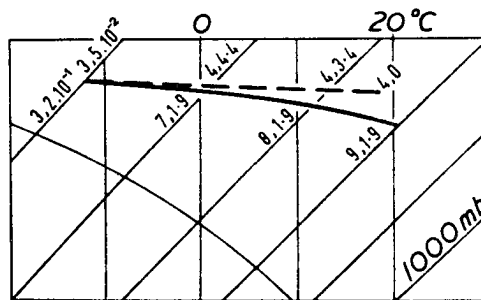
Hookings (1965) derived the equations for heat conduction, conservation of mass and of water for a monodisperse distribution of raindrops assuming steady-state downdrafts and environmental lapse rates. The results of his computations show that the smaller the initial drop radius the greater is the speed of the downdraft produced; the faster downdraft speeds are associated with the lower relative humidities; the greater the mass of liquid water introduced initially the greater the downdraft speed produced. In fact, the downdraft speed at the level where evaporation commences is almost exactly proportional to the mass of liquid water introduced. His results also show that the relative humidity of a parcel increases as it approaches the surface which is not always the case in the actual atmosphere.

Using equations similar to those described above Kamburova and Ludlam (1966) showed that only in an intense rain of small drops did the descent of air in the downdraft approximate to the psuedo adiabatic reference process (see Fig. 2.1) and only closely if the downdraft was weak. If the general lapse rate was approximately equal to the dry adiabatic lapse rate then the microphysics of the evaporation process placed much less restriction on the downdraft magnitude and even in a moderate rain of large drops strong downdrafts might be generated. Correspondingly, the microphysics become unimportant and the descent approximates the saturated adiabatic in the case of extremely weak downdrafts.



Temperature and humidity in *strong* (continuous lines), *moderate* (dashed lines) and *weak* (pecked lines) downdraughts, produced by the evaporation of *intense* (I), *heavy* (H) and *moderate* (m) rains, of uniform initial drop size 0.5 (left) and 2 mm (right). The rainfall intensities at 500 mb are respectively 250, 50 and 5 mm hr⁻¹. The temperature profiles are drawn upon sections of a tephigram limited by the horizontal dry adiabatics corresponding to potential temperatures of 30 and 50°C. The isobars are drawn at intervals of 100 mb. The lowermost curve is the saturated pseudo-adiabatic corresponding to the wet-bulb potential temperature of 18°C, which is preserved in the downdraughts. At each 100 mb level the pairs of figures entered beside the profiles for the strong and the weak downdraughts give the relative humidity in per cent, followed by the drop radius in units of 10⁻² cm in diagrams (a) to (c), and in units of mm in diagrams (d) to (f). In all cases the downdraught air is assumed to be saturated at a temperature of -12.2°C at the 500 mb level.

The vertical air speeds are respectively about 20 (24.8 to 16.8) m sec⁻¹, about 10 (12.4 to 8.4) m sec⁻¹ and about 2 (2.5 to 1.7) m sec⁻¹ in the strong, moderate and weak downdraughts. A more accurate specification of the results is given in Table 1.



Temperature and humidity in downdraughts produced in initially very dry air by the evaporation of rain; dashed line: moderate downdraught (vertical speed about 10 m sec⁻¹, moderate rain of initial drop size 0.5 mm; continuous line: strong downdraught (speed about 20 m sec⁻¹, intense rain of initial drop size 2 mm). The two temperature profiles are drawn upon sections of a tephigram limited by the horizontal dry adiabatics corresponding to potential temperatures of 20 and 50°C. The isobars are drawn at intervals of 100 mb. The lowermost curve is the saturated pseudo-adiabatic corresponding to the wet-bulb potential temperature of 15°C, which is preserved in the downdraughts. At each 100 mb level the pairs of figures entered beside the profiles give the relative humidity in per cent, followed by the drop radius in units of 10⁻² cm (upper curve) and in units of mm (lower curve). In both cases the downdraught of air is assumed to be very dry (R.H. = 3 per cent) at a temperature of -12.2°C at the 500 mb level. The conditions at lower levels are also specified in Table 2, and can be compared with those in Table 1 and Figs. 1 (c) and (d).

Figure 2.1 From Kamburova and Ludlam (1966).

Das and Subba Rao (1972), with the same kind of computations as those used by Kamburova and Ludlam (1966) pointed out that a strong downdraft causes a high rate of adiabatic compression of the descending air and allows only a short time for its liquid water content to evaporate; on the other hand, a given liquid water content composed of a small number of large drops evaporates much less than when it consists of a large number of small drops. A strong downdraft carrying its liquid water content in the form of large drops will tend to remain unsaturated not only when the liquid water content is small, thereby causing a shower of low intensity, but also when a large liquid water content is transported by an intense thunderstorm rainfall.

The evaporation of water drops was considered by Takeda (1966) to be the most important factor in the development of downdrafts although it cannot be completely studied without considering the dynamical effects of compensating currents and gravity waves.

Summarizing, in order for the air to move downward it must either be cooled until it becomes negatively buoyant or be carried down by the fluid motion. The cooling may occur by one of the following processes:

- a) evaporation of rain or hail

Before the formation of the downdraft, the evaporation may take place in entrained dry air from the environment, or if there is a flow under a raining anvil.

- b) melting of ice particles

When hailstones with a radius of 2 mm and water content of 10 gm m^{-3} fall through a layer 2 km in depth (after which they are completely melted), the air in this layer is roughly estimated to be cooled by $1^\circ\text{C} / \text{min}$.

The motion may also be started by

a) drag force of water drops

If each drop is assumed to fall with its terminal velocity which depends upon its size, the air will be subject to the downward drag force which is equal to the total weight of water drops in the air. If liquid water is accumulated in a shallow layer by the fall of raindrops, as was first observed by Donaldson (1961), the air in the layer is subject to considerable downward force.

b) forcing by the spreading out of the surface density current

As will be seen in the next section, the model of Miller and Betts (1977) suggests the existence of an upper level downdraft which is forced to descend by mass continuity due to the spreading out of the lower level downdraft which behaves as a density current.

c) dynamic interaction of cloud with sheared environment

The next section will discuss the results of some simulations in which the downdraft develops in the absence of precipitation as a result of dynamic interaction with a sheared environment.

2.2 Some results from numerical simulations

It appears that in order to numerically simulate the structure of the downdraft, it is necessary to model the precipitation process, that is, to model the conversion from cloud water into rain water. Many authors assume that inside a cloud any excess of water vapor over that required to saturate the air condenses immediately. Similarly, a deficit below saturation is immediately supplied by the evaporation of any available condensed water (Srivastava, 1967; Liu and Orville, 1969; Orville and Sloan, 1970; and Takeda, 1971). A more complete treatment

of the parameterization of rain may be found in Berry (1968), Kessler (1969), and Manton and Cotton (1977).

In Srivastava's (1967) one dimensional model the rain water production term consisted of two parts: the exchange between the vapor field and the raindrops and the exchange between rain water and cloud water. He utilized Kessler's (1969) procedure of parameterizing the autoconversion and accretion processes. His results showed the development of downdrafts proceeding from cloud base down towards the ground and up towards cloud top. However, this downdraft did not spread throughout the cloud. Arnason, et al. (1968) using the same procedure as Srivastava (1967) developed a two dimensional slab-symmetric model for shallow convection. They presented the results of their simulation up to 8 min. and suggested that if the experiment had been continued one would have witnessed the development of a downdraft due to the negative buoyancy of water in cloud and in precipitation.

Takeda (1966) modeled an isolated convective cloud accompanied with rainfall. A forced updraft was always given at lower levels in the atmosphere which was set at rest and accelerated upward or downward by buoyancy forces and by the weight of water drops. The numerical simulation showed that the downdraft was initiated by the weight of raindrops because when it began the cloud temperature was higher than that in the surrounding atmosphere.

Liu and Orville (1969) numerically integrated the equations of motion, conservation of water and thermodynamic energy in a two dimensional slab-symmetric space with vertical wind shear, in a stable incompressible atmosphere, in order to study the effects of precipitation on a model of cumulus cloud initiation and development over mountains.

They illustrated some similarities between precipitating and non-precipitating cases: the downdrafts appeared beneath raining and non-raining clouds, in the last case probably as a result of the dynamic interaction of the cloud and the sheared environment.

Orville and Sloan (1970) extended the region of integration used by Liu and Orville (1969) and showed that downdrafts alongside the maximum updrafts became stronger and created clear areas in the cloud. They concluded that these downdrafts were probably a result of continuity and of the falling precipitation.

Takeda (1971) used a two dimensional slab-symmetric model in which he integrated the hydrodynamic and thermodynamic equations in order to study the effect of the vertical profile of the ambient wind on a precipitating convective cloud. He included the effects of condensation, evaporation, coagulation and break-up of drops. He showed that if the vertical shear in the ambient wind was very weak the current of cold air which spread from the downdraft near the ground pushed potentially warm air in the lower layers in the manner of a cold front. In a strong vertical shear of constant sign the downdraft formed in the downshear side of the cloud. When there was a change of sign of the vertical wind shear in such a way that there was a jet in lower levels and a jet in the opposite direction in upper levels, the pattern of rain water content and the downdraft were displaced to the left of the updraft. Only in this case the downdraft air which fed new upcurrents contributed to the formation of new convective clouds.

The three dimensional model of Wilhemson (1974) although having considerable unstable numerical amplification of gravity waves, showed

that in a moderately sheared structure the downdraft formed to the down-shear side of the cloud.

Moncrieff and Miller (1976) developed a three dimensional model of tropical cumulonimbus convection which featured a close cooperation between the updraft and downdraft circulations. The mathematical formulation is essentially that described in Miller and Pearce (1974) who developed a three dimensional model using pressure as the vertical coordinate. The initial stratification of temperature and moisture for the numerical simulation is that of a radiosonde sounding taken prior to a squall-line observed during VIMHEX-1972. The initial wind field shows a low level easterly jet with a maximum wind speed of 16 m.s^{-1} at 700 mb and westerlies above 300 mb. A single cumulonimbus cell is initiated whose rain stage is characterized by the formation of a downdraft on the upshear side and an extending area of relatively cool air near the surface. The first cumulonimbus cell downdraft extended down from around 700 mb; at later times the downdraft always originated at or below this level and was often only identifiable in the lowest 100-150 mb. Examination of the wet bulb potential temperature (θ_w) of this air confirmed that the air originated at or below 750 mb ($\theta_w \geq 21^\circ\text{C}$), and hence much of the air came from near cloud base. The comparison of Moncrieff and Miller's (1976) results with the results from the two dimensional model of Takeda (1971), initialized with a wind profile showing a low-level jet and a jet in the opposite direction in upper levels, shows some crucial differences particularly on the side in which the downdraft is found and in the slope of the updraft-downdraft. In order to understand this difference, one should examine closely the initial conditions in both cases. In the initial conditions of Moncrieff and Miller (1976),

the atmosphere is quite unstable with a lifting condensation level at 850 mb, so that a cloud with base at this level and top say, at 400 mb, will travel faster than the flow at lower levels and so there will be inflow at lower levels in the front of the cloud and outflow at upper levels in the rear. The downdraft will be able to form and spread under the updraft and this will happen in the upshear side of the cloud.

Takeda's (1971) initial conditions show a less unstable atmosphere with the lifting condensation level at 775 mb; the wind profile shows a jet at this level and the wind changes sign at 650 mb. A cloud with base at the LCL and top at 400 mb would travel with the mean speed which should be very close to zero and so there is an inflow at lower levels in the back of the cloud and an outflow as before at upper levels in the back of the cloud. The downdraft is then able to form under the sloping updraft at the downshear side of the cloud. This is characteristic of middle latitude storms while Moncrieff and Miller (1976) initialization and results are typical of tropical travelling storms.

Using VIMHEX-72 data and numerical simulation, Miller and Betts (1977) distinguished two classes of downdrafts: a "cell" and a "system" downdraft representing different dynamical mechanisms and different thermodynamic effects, the former evaporatively driven tending to produce warming and drying of the air. It appears that the forced downdraft is related to the dynamics of a density current, i.e. the spreading current and its propagation drives a circulation involving air other than the cooled air alone. The sounding data appears to confirm the presence of a warm system or mesoscale unsaturated downdraft which is being forced to descend over the spreading "cold pool".

Haman and Niewiadomski (1976) developed a one dimensional, purely buoyant model in which updraft and downdraft interact due to entrainment. The numerical experiments showed that a rainfall of realistic intensity is not likely to maintain a steady, cold downdraft down to the ground unless the hydrostatic stability of the environmental air is very low. Kamburova and Ludlam (1966) calculated the buoyancy corresponding to a temperature difference of 1°C between the downdraft and its environment and also found out that the hydrostatic stability was low. Haman and Niewiadomski (1976) showed that the downdraft in the upper and central parts of the cloud can be maintained by entrainment of cloudy air from the neighboring updraft; nevertheless, such downdrafts did not reach the ground. Fairly realistic cold downdrafts may form if additional supplies of easily evaporable water is allowed. A source of such a supply may be attributed to the updraft provided that the updraft-downdraft interface is slanted and that the updraft (overlying the downdraft) contains sufficient amounts of liquid water in small droplets.

The spectral mass flux associated with the downdraft has been derived by Johnson (1976) using a spectral model analogous to the one derived by Arakawa and Schubert (1974) for the updraft. He computed the entrainment parameters assuming that the downdraft is saturated. A correction of subsaturation was not applied, as he pointed out, since direct measurements of the degree of subsaturation in tropical cumulonimbus downdrafts was lacking. He points out that in the theories for the parameterization of cumulus, in particular those of Ooyama (1971) and Arakawa and Schubert (1974), only the effect of updrafts are considered and that the neglect of the downdraft leads to predictions of excessive warming and drying in the lower troposphere.

2.3 Conclusion

Diagnostic models and observational studies agree in that the main downdraft air originates at or below 700 mb although some sinking motion required by mass continuity may be observed in higher altitudes. The maintenance of the downdraft current is mostly associated with evaporation and drag force of falling raindrops.

The numerical simulations based on the integration of the primitive equations have been successful in obtaining the initiation of the downdraft usually by the weight of water drops and by the required continuity of mass. The development of new cells from the convergence along the leading edge of the downdraft air has also been obtained in moderately sheared environments. But one of the main things that has been lacking in most of the numerical simulations is a comparison between their results and actual observations: the amounts of rainfall or the maximum rainfall intensities as well as downdraft speeds which may be encountered in a system which develops from given initial conditions.

The following chapters will introduce a set of equations analogous to those used by Kamburova and Ludlam (1966) which will be used in order to define a microphysical parameter which will specify a relationship between rainfall intensities, downdraft speeds and drop spectra.

III. THE EVAPORATION IN THE DOWNDRAFT CURRENT

The downdraft current is known to take place under unsaturated conditions even if raindrops are being evaporated in it. The first law of thermodynamics may be written as

$$c_p \frac{d \ln \theta}{dt} = \frac{\dot{H}}{T} \quad (3.1)$$

where θ is the potential temperature, c_p is the specific heat at constant pressure, T is temperature, t is time and \dot{H} is the diabatic heating rate which in the case where evaporation of drops is taking place is given by

$$\dot{H} = -L \frac{d\chi}{dt} \quad (3.2)$$

where χ is the water vapor mixing ratio and L is the latent heat of condensation. Introducing Eq. (3.2) into Eq. (3.1) and integrating the resulting expression from a state (θ, χ) to one in which the air is completely dry $(\theta_E, 0)$ θ_E being the equivalent potential temperature we get

$$\theta_E = \theta \exp \left(- \int_{\chi}^0 \frac{L}{c_p T} d\chi \right) \quad (3.3)$$

so that the changes in temperature and mixing ratio under the evaporation process will take place with a constant θ_E , even if the air is subsaturated.

The evaporated water vapor from a raindrop will be diffused to the ambient air and the changes in the environment due to latent heat release will be assumed to occur under constant θ_E .

3.1 Governing equations

The equations which will be presented may use a distribution of single-sized raindrops in which the radius of the single drop represents some sort of mean, or, a drop-spectrum may be defined by some analytical expression. Both procedures will be presented here. The first one was used by Kamburova and Ludlam (1966) and by Das and Subba Rao (1972); the second one, by Syono and Takeda (1963), Takeda (1970), Srivastava (1967), among others. A one dimensional kinematical approach will be followed, in which the vertical velocity is specified, rather than computed.

3.1.1 Single drop case

The growth or decay of individual drops mass is described by the diffusion equation

$$\frac{dm}{dt} = 4 \pi r D \rho_v s C_v \quad (3.4)$$

where m is the mass of a drop of radius r

$$s = \frac{x - x'_w}{x} = - \frac{\Delta x}{x} \quad (3.5)$$

x is the water vapor mixing ratio

x'_w is the temperature vapor mixing ratio at the wet bulb temperature T_w

ρ_v is the vapor density

D is a coefficient of diffusion of water vapor in air and is given by, according to Kinzer and Gunn (1951)

$$D = 0.22 \text{ cm}^2 \text{ s}^{-1} \left(\frac{T_w}{273.2^\circ\text{K}} \right)^{1.75} \left(\frac{1000 \text{ mb}}{p} \right) \quad (3.6)$$

C_v is a ventilation coefficient in order to take into account the motion of drops through the air.

Eq. (3.4) may be rewritten to give the growth of an individual drop

$$r \frac{dr}{dp} = \frac{C_v D \Delta x}{\rho_L g (V_T + w)} \quad (3.7)$$

where ρ_L is the liquid water density
 g is the gravity
 V_T is the terminal velocity of a drop of radius r
 w is the downdraft vertical velocity
 p is pressure as a vertical coordinate.

Some conservation equations will now be presented following Kamburova and Ludlam (1966). The continuity equation is

$$\frac{\partial \rho}{\partial t} = \nabla \cdot (\rho \underline{V}) \quad (3.8)$$

where ρ is the air density and \underline{V} is the three dimensional velocity vector, $\underline{V} = (u \underline{i}, v \underline{j}, w \underline{k})$. For uni-dimensional steady-state vertical flow Eq. (3.8) may be written as

$$\frac{d}{dz} (\rho w) = 0. \quad (3.9)$$

or by the use of the hydrostatic equation,

$$\frac{d}{dp} (\rho w) = 0. \quad (3.10)$$

Eq. (3.9) or (3.10) imply that as the air descends and its density is increased it must suffer a deceleration to satisfy the continuity of mass. This deceleration will be small so that the vertical velocity will not be zero when the ground is reached. In Section 3.1.3, another procedure will be presented in order to avoid this problem.

The equation for the conservation of raindrop number in the absence of break-up and collection is

$$\frac{\partial N}{\partial t} = - \nabla \cdot [N (\underline{v} + v_T \underline{k})] \quad (3.11)$$

where N is the number of drops per unit volume. With the same assumptions as in the derivation of Eq. (3.9), we may write Eq. (3.11) as

$$\frac{d}{dz} [N (v_T + w)] = 0 \quad (3.12)$$

or

$$\frac{d}{dp} [N (v_T + w)] = 0. \quad (3.13)$$

As the air is decelerated as imposed by Eq. (3.9) or (3.10), the number of raindrops per unit volume will be slightly increased.

The total mass of water per unit volume is given by

$$\rho_X + \rho_R \quad (3.14)$$

where ρ_R is the rain density which is given by

$$\rho_R = \frac{4}{3} \pi r^3 \rho_L N. \quad (3.15)$$

The conservation of mass of water may then be written, under the same assumptions used in order to derive Eq. (3.9) and (3.12)

$$\frac{d}{dz} [\rho_X w + \rho_R (V_T + w)] = 0 \quad (3.16)$$

or

$$\frac{d}{dp} [\rho_X w + \rho_R (V_T + w)] = 0. \quad (3.17)$$

Introducing Eq. (3.7) into Eq. (3.17) and using Eq. (3.10, 3.13 and 3.15) we get

$$\frac{d\chi}{dp} = - \frac{4\pi D \Delta\chi r NC_v}{\rho g w} . \quad (3.18)$$

This equation gives the change of mixing ratio with height due to evaporation. If the air is just saturated, $\Delta\chi$ (which is the difference between the mixing ratio at the air temperature and at the wet bulb temperature) will be zero and so, no change in the mixing ratio of the descending parcel will occur.

Kamburova and Ludlam (1966) used Eq. (3.7), (3.9), (3.12) and (3.16), plus the assumption that the evaporation is taking place under constant equivalent potential temperature, to derive temperature and moisture profiles for different raindrop radii, downdraft speeds and rainfall intensities (Fig. 2.1). The same procedure will be followed here [substituting Eq. (3.7) by Eq. (3.18)] but the initial conditions will be chosen in such a way as to reproduce actual temperature and moisture structures in some VIMHEX-1972 soundings. This is discussed further in sections 3.2 and 3.3. The computational scheme may be seen in Fig. 3.1.

3.1.2 Drop spectrum case

The conservation equations will now be written taking into account the size distribution of raindrops. The continuity equations (Eq. 3.9 or 3.10) remain the same. Conservation of raindrop number

$$\frac{d}{dp} [n(r) (V_T(r) + w)] = 0 \quad (3.19)$$

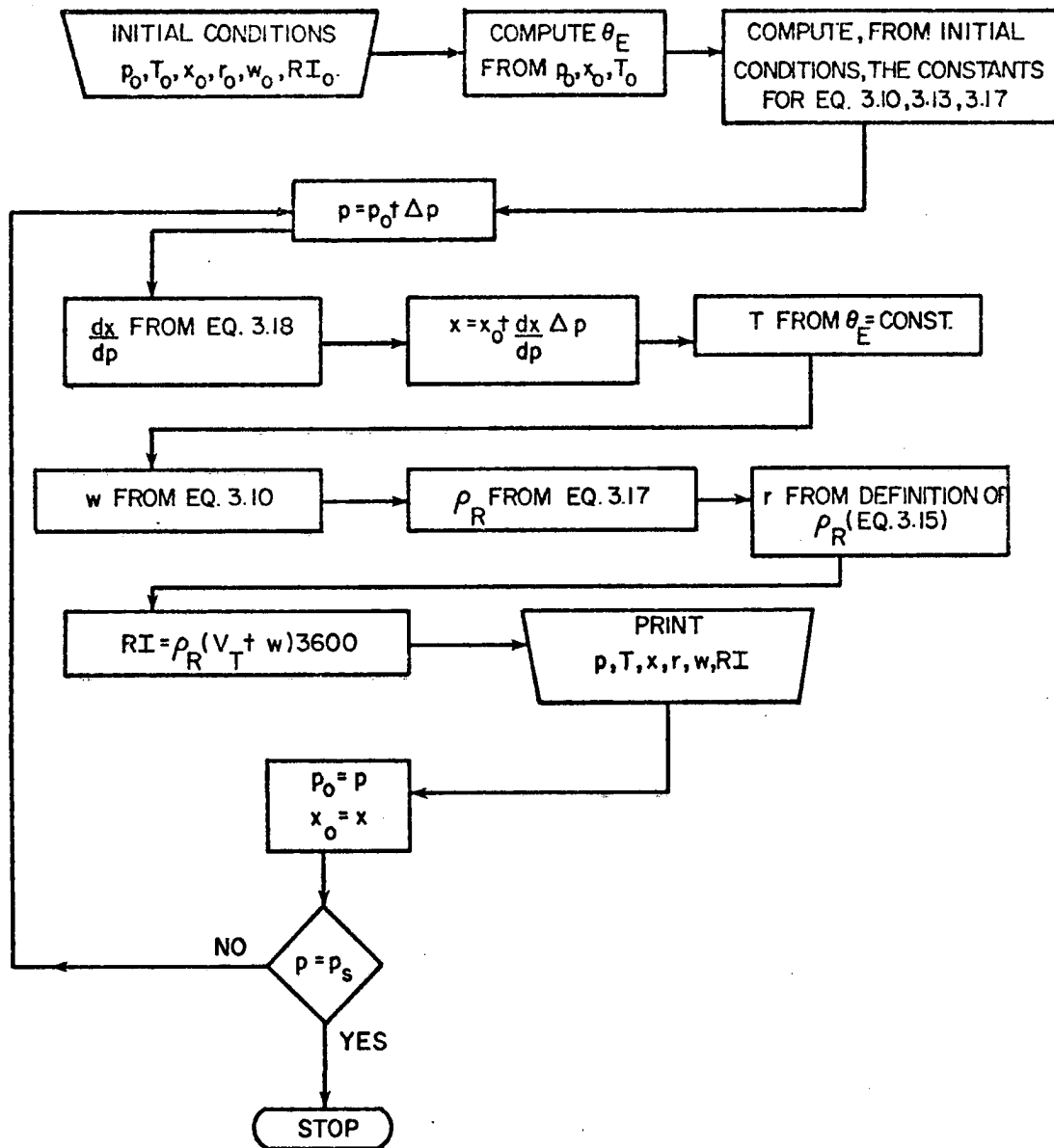


Figure 3.1. Computational scheme for the single drop approach.

where $n(r)$ is the number of drops per drop radius interval $(r - \delta r/2, r + \delta r/2)$, per unit volume. In this case $n(r)$ is conserved but not the total number of raindrops.

Continuity of the mass of water is given by

$$\frac{d}{dp} [\rho_X w + \rho_R (\bar{V}_T + w)] = 0 \quad (3.20)$$

where

$$\rho_R = \int_0^{\infty} \frac{4}{3} \pi r^3 \rho_L n(r) dr \quad (3.21)$$

and \bar{V}_T is the mean of effective terminal velocity.

Introducing as before, Eq. (3.7) into Eq. (3.20) we get

$$\frac{dX}{dp} = - \frac{4 \pi D \Delta X}{\rho g w} F \quad (3.22)$$

where

$$F = \int_0^{\infty} r n(r) C_V(r) dr. \quad (3.23)$$

Thus, we can calculate the vertical gradient of the mixing ratio if we know w and F [c.f. Eq. (3.18)].

In order to calculate F in Eq. (3.23), the functions $n(r)$ and $C_V(r)$ have to be known. The raindrops will be assumed to be size distributed

following an inverse exponential law in accordance with Marshall and Palmer (1948)

$$n(r) = n_0 \exp (-2\lambda r). \quad (3.24)$$

According to Kessler (1969), n_0 is constant and λ is a parameter which specifies the type of precipitation. Manton and Cotton (1977), on the other hand, suggested using λ constant, essentially independent of the detailed environment, and allowing n_0 to vary with the rainfall intensity. In the first case, the variation of λ with the type of rain (thunderstorm, orographic, etc.) is governed by two parameters b and β

$$\lambda = 3.67 / D_0 \quad (3.25)$$

where

$$D_0 = b [RI_{(w=0)}]^\beta \quad (3.26)$$

or

$$D_0 = b (\rho_R V_T)^\beta. \quad (3.27)$$

D_0 is the median volume diameter which divides the distribution into parts of equal water content. $RI_{(w=0)}$ is the rainfall intensity with no vertical velocity. Table 1 shows the variation in λ for each kind of

RI $\lambda(m^{-1})$ (mm/ hr)	I	II	III	IV	V	VI	VII	VIII
6	2662	3074	3058	5974	4728	2213	2267	2768
10	2296	2651	2369	4870	3914	2008	2210	2487
20	1878	2168	1675	3691	3028	1760	2135	2150
30	1669	1928	1367	3138	2607	1630	2092	1974
40	1536	1773	1184	2797	2343	1543	2062	1859
50	1439	1662	1059	2558	2158	1479	2039	1774
60	1365	1577	967	2378	2017	1429	2021	1707
70	1306	1508	895	2236	1905	1387	2005	1653
80	1256	1450	837	2120	1813	1353	1992	1607
90	1214	1402	790	2022	1736	1323	1980	1568
100	1177	1360	749	1939	1670	1296	1970	1533

b	β	Type of Rain / Location	Author	
I.	0.82	0.29	thunderstorm	Sivaramakrishnan (1961)
II.	0.71	0.29	continuous rain with melting band	
III.	0.49	0.50	warm layer cloud	
IV.	0.30	0.40	warm orographic: in cloud	Blanchar (1953)
V.	0.40	0.37	warm orographic: at cloud base	
VI.	1.18	0.19	non orographic rain	
VII.	1.48	0.05	heavy showers / Illinois	Jones (1956)
VIII.	0.91	0.21	continuous rain / Canada	Marshall and Palmer (1948)

Table 1. Variation of λ as a function of rainfall intensity and type of rain as specified by the parameters b and β .

rain for different values of b and β listed by Mason (1971). As may be seen in that table, λ varies strongly from one type of rain to another for a fixed rainfall intensity. This approach has the inconvenience that the parameters b and β have to be known previously and the data that will be used here do not provide such information. In that case, some kind of decision has to be made in the sense of using one or another type of b and β parameters in Table 1. In the Manton and Cotton (1977) parameterization n_0 is given by the definition of rainfall intensity, which is the following (in mm hr.⁻¹)

$$R_I = 3600 \rho_R (\bar{V}_T + w) \quad (3.28)$$

where ρ_R is obtained by the integration of the right hand side of Eq. (3.21) as

$$\rho_R = 8 \pi n_0 \rho_L (2\lambda)^{-4}. \quad (3.29)$$

In this case, as will be seen later, there is a need to tune the value of λ to the data.

In section 3.3.1 the results from the two approaches will be presented and discussed.

The ventilation coefficient may be written as, according to Frossling (1938)

$$C_v = 1 + 0.22 R_e^{1/2} \quad (3.30)$$

where R_e is the Reynolds number

$$R_e = \frac{2 \rho r V_T}{\eta} \quad (3.31)$$

η being the viscosity coefficient. The terminal velocity resulting from a fitting done by Manton and Cotton (1977) is

$$V_T(r) = 2.13 \left(\frac{\rho_L}{\rho} g r \right)^{1/2}. \quad (3.32)$$

Substituting Eq. (3.32) and (3.31) into Eq. (3.30) we obtain an approximate expression for the ventilation coefficient as a function of raindrop radius

$$C_v(r) = 1 + 1160 r^{0.75} \quad (3.33)$$

in which r is given in meters. Table 2 shows a comparison between the result from Eq. (3.33) and the results obtained by Frossling (1938) and Kinzer and Gunn (1951). The differences are greater for very small drops but in that case, there is poor agreement between Kinzer and Gunn

r mm	C_V from Eq. (3.33)	Kinzer & Gunn (1951) Frossling (1938)	
0.2	3.0	2.8	2.4
0.5	4.9	4.5	4.6
1.0	7.5	7.4	7.5
1.5	9.8	9.8	9.8
2.0	12.0	13.8	11.7

Table 2. Ventilation coefficient as a function of drop radius as given by Eq. 3.33, by Frossling (1938) and Kinzer and Gunn (1951).

(1951) and Frossling (1938). Eq. (3.33) gives a maximum error of 13% in comparison with Kinzer and Gunn values.

Substituting Eqs. (3.24) and (3.33) into Eq. (3.23) we get

$$F = n_0 [(2\lambda)^{-2} + 1160 \Gamma(2.75) (2\lambda)^{-2.75}] \quad (3.34)$$

where λ has to be given in M K S units and $\Gamma(2.75) = 0.91906$, Γ being the gamma function. The total number of raindrops is given by

$$N = n_0 / \lambda. \quad (3.35)$$

The mean of effective terminal velocity which appears in Eqs. (3.20) and (3.28) is given in the Kessler parameterization by

$$\bar{V}_T = 1.94 V_T(r_m) \quad (3.36)$$

where $r_m = 1/2 \lambda.$ (3.37)

The computational scheme may be seen in Fig. 3.2.

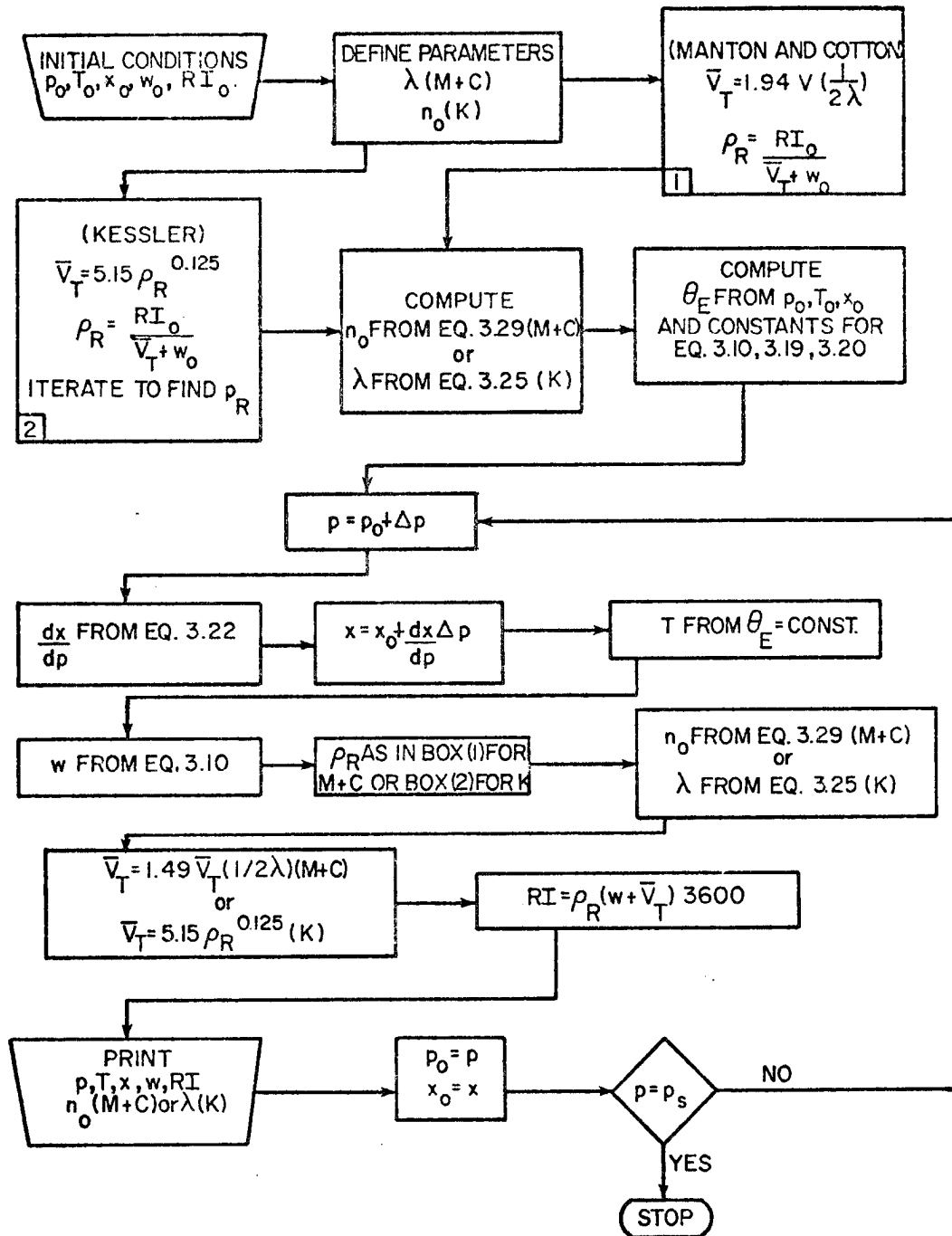


Figure 3.2. Computational scheme for the drop spectrum approach.

The effects of break-up are not being explicitly considered here. The inclusion of a Marshall-Palmer spectrum will, nevertheless, force the existence of very small drops at each level even if the evaporation would have depleted this part of the spectrum. Thus, an implicit break-up process is included.

The effect of melting of ice crystals will not be included. The reason for this is that in most of the cases studied here the outflow in upper levels is taking place behind the travelling storm so that the ice crystals formed in these upper levels (the freezing level is between 600-500 mb) are carried away from the storm and thus, fall in clear air. Hall and Pruppacher (1976) have shown that ice crystals falling from cirrus clouds in an unsaturated environment with relative humidities with respect to ice of less than 70% may survive distances of up to 2 km, for a wide range of initial sizes. If the ice crystals are forming around 400-300 mb and if they are falling in an unsaturated downdraft, if they survive for a distance of 3 km, this brings them to around 600 mb. Reaching the freezing level the decrease in the size of the ice crystals may be enhanced by melting so that at the 700 mb level there will not be any ice-crystal effect; since all calculations performed here start at or below 700 mb there will be no need to consider this effect.

3.1.3 Equations with a constant divergence profile

The equations of section 3.1.1 and 3.1.2 have been derived under the assumption of conservation of mass as given by Eq. (3.9). This equation assumes a small deceleration ($\sim 20\%$) as the parcel reaches the ground. A realistic profile would show the downdraft speed approaching

zero at the surface but this is not handled by Eq. (3.10). There is a way, however, of specifying the vertical profile of w by introducing a constant horizontal divergence in such a way that Eq. (3.8) may be written under steady state conditions as

$$\frac{\partial}{\partial z} (\rho w) = - \rho \text{Div} \quad (3.38)$$

where Div is the horizontal velocity divergence which is assumed to be constant with height. This equation may be rewritten as

$$\frac{\partial}{\partial p} (\rho w) = \frac{\text{Div}}{g} . \quad (3.39)$$

Eq. (3.39) may be integrated from the surface (p_s) to a level p , to give

$$w = \frac{\text{Div}}{\rho g} (p - p_s). \quad (3.40)$$

The conservation of raindrop number and of the mass of water may now be written in a similar way as Eq. (3.38)

$$\frac{\partial}{\partial z} [N (V_T + w)] = - N \text{Div} - \underline{V} \cdot \nabla_H N \quad (3.41)$$

$$\text{and } \frac{\partial}{\partial z} [\rho_X w + \rho_R (V_T + w)] = - (\rho_X + \rho_R) \cdot \text{Div} - \underline{V} \cdot \nabla_H (\rho_X + \rho_R) \quad (3.42)$$

with analagous equations in the drop spectrum case. This equation may be simplified by putting the horizontal gradients of N and of $\rho_X + \rho_R$ equal to zero. Clearly this assumption will only be valid near the center of the rain area. We have indeed replaced the assumption involved in Eq. (3.9) of a constant ρw with the consequent non-zero ground vertical velocity by one in which the rain area is homogeneous but divergent. In section 3.3 the results obtained using both approaches will be compared.

Eqs. (3.41) and (3.42) may now be written as

$$\frac{\partial}{\partial p} [N (V_T + w)] = \frac{N}{\rho} \frac{\text{Div}}{g} \quad (3.43)$$

$$\text{and } \frac{\partial}{\partial p} [\rho_X w + \rho_R (V_T + w)] = \frac{\rho_X + \rho_R}{\rho} \frac{\text{Div}}{g} . \quad (3.44)$$

Eq. (3.7) may be introduced in Eq. (3.44) to give

$$\frac{\partial X}{\partial p} = - \frac{4 \pi D \Delta X}{\rho g w} r N C_v \quad (3.45)$$

which is again Eq. (3.18).

Eqs. (3.43) and (3.44) may be integrated from an initial level p_I to a level p

$$N (V_T + w) = N_I (V_T + w_I) + \frac{\text{Div}}{g} \int_{p_I}^p \frac{N}{\rho} dp \quad (3.46)$$

and

$$\begin{aligned} \rho_X w + \rho_R (V_T + w) &= \rho_I x_I w_I + (\rho_R)_I (V_T + w_I) \\ &+ \frac{\text{Div}}{g} \int_{p_I}^p \frac{\rho_X + \rho_R}{\rho} dp. \end{aligned} \quad (3.47)$$

3.1.4 Parameterization of the evaporation equation

It is unusual to have precise information about downdraft speeds, rainfall intensities and drop sizes and their variation with height from experimental data so that some kind of parameterization is needed to avoid their specification. With this in mind, the evaporation equation (Eq. 3.18, 3.22 and 3.45) may be rewritten in the following form

$$\frac{dx}{dp} = \frac{\Delta x}{\pi_E} = \frac{x' w - x}{\pi_E} \quad (3.48)$$

where π_E may be considered a pressure scale for evaporation, being equal to

$$\pi_E = - \frac{\rho g w}{4 \pi D N r C_v} \quad (3.49)$$

or

$$\pi_E = - \frac{\rho g w}{4 \pi D F}. \quad (3.50)$$

For typical values such as $\rho = 0.98 \text{ kg}\cdot\text{m}^{-3}$, $D = 0.29 \times 10^{-4} \text{ m}^2\cdot\text{s}^{-1}$, $N = 1620 \text{ m}^{-3}$, $r = 0.8 \text{ mm}$, $w = 2 \text{ m}\cdot\text{s}^{-1}$ ($RI = 96 \text{ mm}\cdot\text{hr}^{-1}$) and $C_v = 6.4$, Eq. 3.49 gives $\pi_E = 6354 \text{ Pascal}$ or 63.5 mb .

The definition of π_E in Eqs. (3.49) and (3.50) suggests that a family of conditions may provide the same variation of mixing ratio with height provided the ratio in the right hand side of Eqs. (3.49) or (3.50) is the same. It also suggests that one may avoid the direct specification of (RI, w, r) by writing

$$\pi_E = \pi_E(p). \quad (3.51)$$

In section 3.3 we will calculate π_E as a function of (RI, w, r) and then fit to the result a function of pressure. Once the dependence expressed by Eq. 3.51 is established, the computational scheme may be simplified as follows:

- 1) given $p_I, T_I, x_I \rightarrow \Delta x_I$ and $\pi_{E_I} = (p_I)$
- 2) $\left(\frac{dx}{dp}\right)_{I+1} = \frac{\Delta x_I}{\pi_{E_I}} \rightarrow x_{I+1} = x_I + \left(\frac{dx}{dp}\right)_{I+1} \Delta p$
- 3) from $\theta_E = \text{const.} \rightarrow T_{I+1}$
- 4) $I = I + 1$, go back to 2) until final level is reached.

As may be noted, there is no need to go into the details of conservation equations.

Eq. (3.48) may be rewritten as

$$\frac{d}{dp} \Delta x + \frac{1}{\pi_E(p)} \Delta x = \frac{d}{dp} x'_w. \quad (3.52)$$

The left hand side of Eq. (3.52) is the variation of mixing ratio along a saturated adiabat which may be considered a constant from 750 mb to the surface (mean/standard deviation = 37) and equal to 2.2 (g/kg)/100 mb. With this simplification, Eq. (3.52) is a first-order non-homogeneous differential equation which may be solved analytically once the dependence of $\pi_E(p)$ is given.

Eq. (3.48) may be considered analagous to an "entrainment" relationship in the sense that the downdraft air is gaining water vapor from the evaporating raindrops with the evaporation coefficient (similar to an "entrainment" coefficient) being equal to $1/\pi_E$. As will be pointed out later, the form of Eq. (3.48) will be particularly useful for modelling purposes. The solution of Eq. (3.52) for $\pi_E(p)$ equal to a constant will be examined in the next chapter with special attention to the asymptotic value which is reached when $(p - p_I)$ becomes greater than π_E .

3.2 Initial conditions of temperature and moisture

The data that will be examined using the equations derived in section 3.1 is from the second Venezuelan International Meteorological and Hydrological Experiment (VIMHEX-1972). A description of the

experimental design may be found in Betts (1976). Basically, sequences of soundings were launched (every 65-100 min) whenever significant radar activity was observed. In general, a line section of soundings were obtained depicting the atmospheric structure in front of, inside and behind a raining, convective system which passed over the observation site (Carrizal, Venezuela, $9^{\circ} 22.8'N$, $66^{\circ} 55.0'W$). The experiment was performed during the rainy season (May 22 - September 6, 1972) although this summer was the driest one recorded at Carrizal. The initial conditions include an initial level with its temperature and mixing ratio, downdraft speed, rainfall intensity and size of raindrops. The initial pressure, temperature and mixing ratio will be fixed, the other three conditions, downdraft speed, rainfall intensity and size of raindrops, will be regarded as variables which will be adjusted in order to obtain different profiles of temperature and mixing ratio.

3.2.1 Conditions corresponding to Betts' (1976) model

We will follow the model presented in Betts (1976) which assumes that the convective system removes a surface layer with thickness Δp which ascends in updrafts and replaces it by the layer above which descends in downdrafts. Fig. (3.3) shows a scheme of this model. The thickness Δp was calculated, for all soundings referred to here, by Betts (1976), and is a good approximation of the LCL of the "before" sounding. In Fig. (3.3), p_I , T_I , x_I are the layer averaged values in the upper layer before the storm while p_F , T_F , x_F , are the layer averaged values for the lower layer after the storm.

We assume, following Betts (1976), that the upper layer with properties p_I , T_I , x_I , follows a downdraft trajectory through the storm and

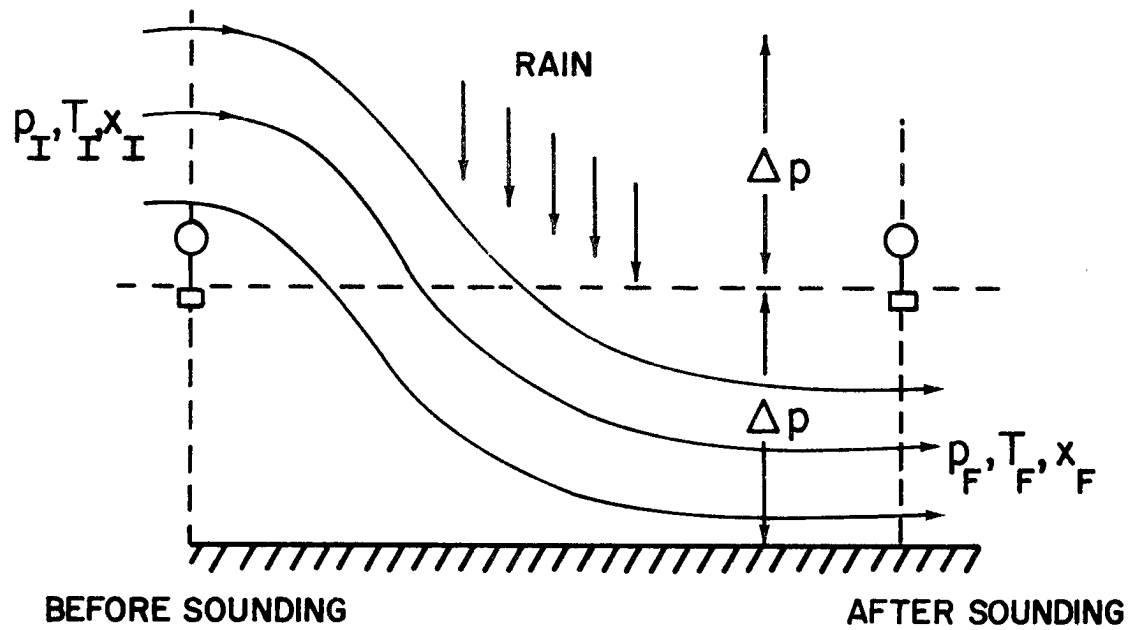


Figure 3.3. Downdraft trajectory according to Betts (1976) model.

leaves with properties p_F , T_F , x_F . The variables (w , RI , r) in the model of section 3.1 will be adjusted to match these two end conditions.

Table 3 lists the values of (p_I, T_I, x_I) and (p_F, T_F, x_F) for 24 pairs of before-after soundings. It may be noted that in most of the storms there were two or three "after" soundings. The mean "before" and "after" soundings are the same ones used by Betts (1976): "These averages were generated by a specific technique designed to preserve the two model layers. The sounding pressures were transformed to a coordinate (see Fig. 1.1)

$$\hat{p} = \frac{p_0 - p}{\Delta p}$$

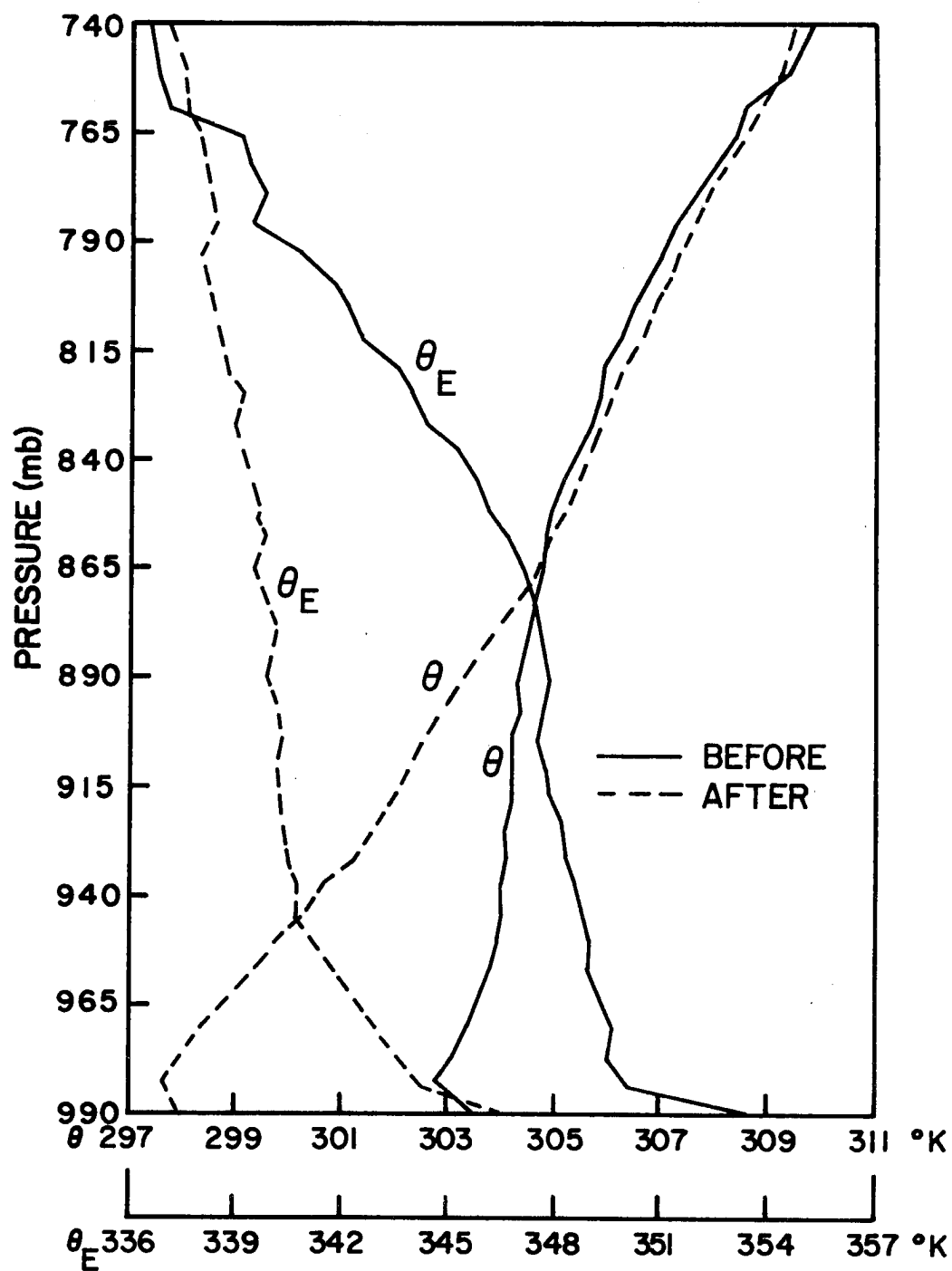
before interpolating the data to intervals of 0.05 in \hat{p} from 0 to 2.0 and then averaging the "before" and corresponding "after" soundings." The profiles of θ and of θ_E for the mean "before" and "after" soundings may be seen in Fig. (3.4)

3.2.2 Conditions for a constant θ_E sounding

A few soundings were launched inside the downdraft or very close to it in such a way that they show a deep layer of almost constant θ_E . The initial conditions of pressure, temperature and moisture were taken, in this case, as those at the top of the layer of constant θ_E . The variables (RI , w , r) were then adjusted in order to match the profiles of temperature and moisture in the given sounding as close as possible.

Before					After				
Sound	p _I	T _I	x _I	θ _E	Sound	p _F	T _F	x _F	θ _E
no.	mb	°C	g/kg	°K	no.	mb	°C	g/kg	°K
Mean	792	13.9	11.3	340.8	Mean	924	21.4	13.4	340.5
59	855	17.6	13.6	344.4	60	945	21.9	15.3	344.4
59	870	18.5	14.2	345.5	61	950	21.8	15.9	345.5
81	735	10.9	9.5	339.2	82	905	21.2	12.2	338.9
81	720	8.9	9.5	338.8	83	900	20.4	12.2	338.5
100	810	15.2	12.7	344.2	101	930	20.9	15.0	343.9
100	765	11.9	8.9	334.7	102	915	20.3	11.9	335.9
116	825	17.0	11.9	342.2	117	935	23.0	13.8	342.4
120	765	13.2	10.9	342.2	121	915	20.6	14.2	342.9
120	930	24.4	15.7	350.2	122	970	23.7	17.5	350.3
120	825	17.2	13.3	346.6	123	935	23.1	15.3	346.9
131	870	18.6	14.2	345.6	132	950	23.9	15.2	346.0
131	840	17.0	13.0	343.7	133	940	23.1	14.5	344.0
176	735	10.7	9.5	339.0	177	905	18.6	13.4	339.3
176	870	20.7	13.5	346.1	178	950	22.5	15.7	345.7
192	795	14.0	11.4	340.8	193	925	21.2	13.8	341.3
192	855	18.0	13.8	345.4	194	945	22.4	15.5	345.6
203	765	12.3	8.8	334.9	204	915	19.9	11.8	335.1
226	840	17.7	11.5	340.1	228	940	22.0	13.5	339.8
241	735	10.5	9.1	337.5	242	905	21.2	12.0	338.3
241	735	10.5	9.1	337.5	243	905	19.9	12.5	338.2
312	750	11.7	10.0	339.7	317	910	18.4	13.6	339.1
312	705	9.1	7.9	336.3	318	895	19.2	11.7	336.2
324	735	9.8	9.1	336.7	325	905	18.1	12.8	337.0
324	840	16.6	13.0	343.2	326	940	23.7	14.1	343.6

Table 3. Initial and final layer averaged conditions for the mean soundings and for 24 pairs of before-after soundings. For a given system there is only one before sounding but there may be one, two or three after soundings.



3.4. Potential temperature and equivalent potential temperature for the mean "before" and "after" soundings.

Only three soundings were found to have a deep layer of constant θ_E , their initial level conditions being those of Table 4.

3.3 Required rainfall intensities, downdraft speeds and drop distributions

This section will present the required rainfall intensities, downdraft speeds and drop distributions needed to match the conditions expressed in sections 3.2.1 and 3.2.2. A comparison between the single-drop and drop spectrum approaches will be performed and also a comparison between the constant mass flux and constant horizontal divergence approaches.

3.3.1 Results for the mean "before" and "after" conditions (model Fig. 3.3)

As pointed out in section 3.1.4 (Eq. 3.50, 3.51) a family of conditions in (RI, w, r) may specify the same profile of μ and consequently of mixing ratio. Since we do not have information about drop sizes or drop spectra, we assumed different values for these variables and then varied (RI, w) to match the final conditions p_F, T_F, x_F for the mean sounding as discussed in section 3.2.1. Fig. 3.5 shows the initial rainfall intensities and downdraft speeds for the single drop case for $r = 0.2, 0.5, \text{ and } 1.0 \text{ mm}$ (continuous lines); for the Kessler parameterization for several pairs of b and β (Eq. 3.27) listed in Table 1 (heavy dashed lines); and for the Manton and Cotton parameterization for $r_m = 0.27 \text{ mm}$ (lightly dashed line). Some of the curves in Fig. 3.5 do not seem to be realistic, either because very low downdraft speeds are associated with very high rainfall intensities (e.g. "heavy showers", $r_m = 0.27 \text{ mm}$, $r = 1.0 \text{ mm}$) or high downdraft speeds associated with very low rainfall intensities (e.g. $r = 0.2 \text{ mm}$). The "thunderstorm" curve presents an

Sound	p_I	T_I	x_I	θ_E
no.	mb	°C	g/kg	°K
82	740	10.0	9.1	336.3
317	780	12.2	10.6	338.2
325	730	8.7	9.0	335.7

Table 4. Initial conditions for the soundings which had a reasonably deep layer of constant θ_E . The conditions shown refer to the top of the constant θ_E layer.

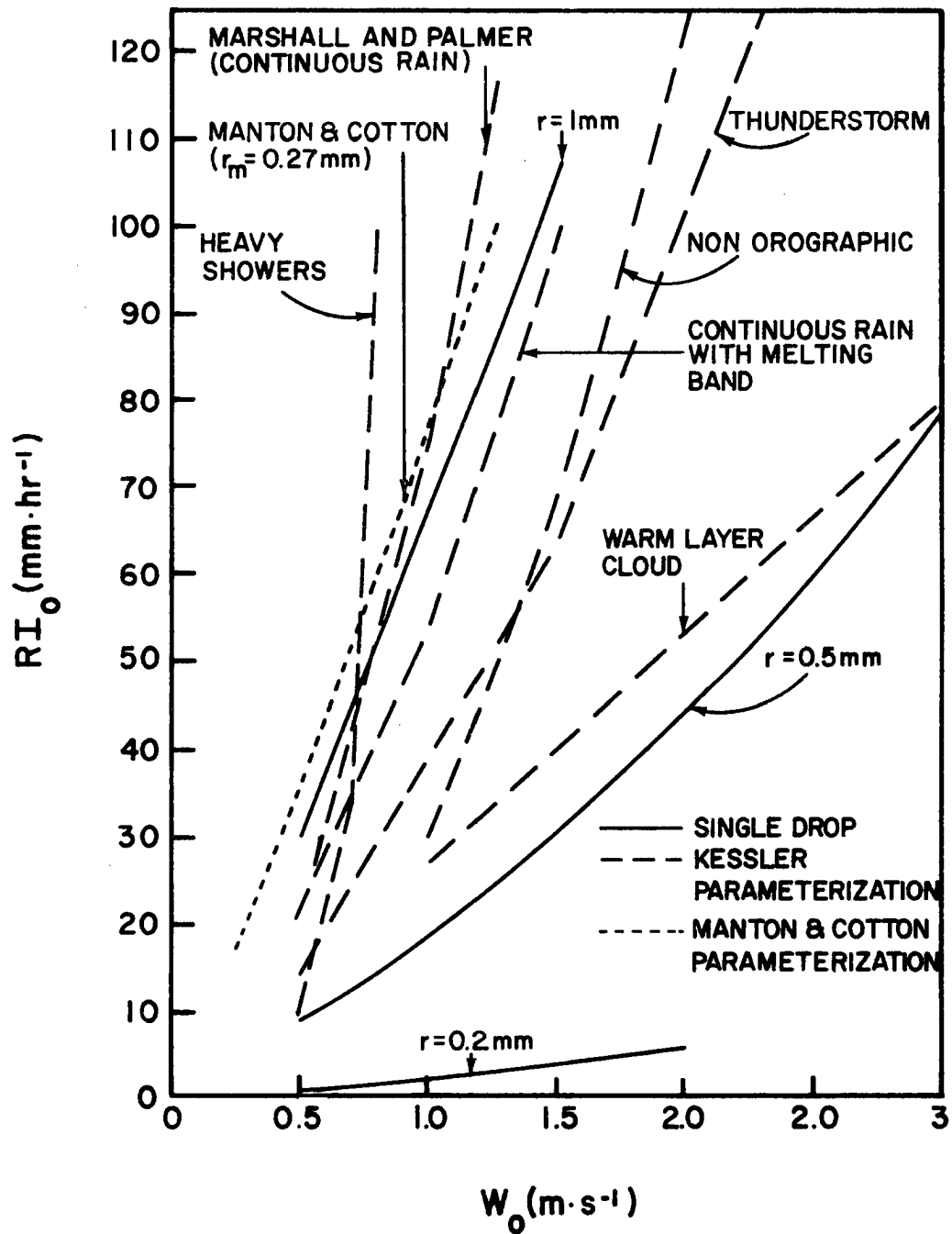


Figure 3.5. Initial rainfall intensities and downdraft speeds for different drop distributions.

association of realistic conditions (e.g. $100 \text{ mm} \cdot \text{hr}^{-1}$ with a downdraft speed of $2 \text{ m} \cdot \text{s}^{-1}$) so it may be used as a reference in order to select r_m in the Manton and Cotton parameterization and the size of the single drop. In Fig. 3.6 it may be seen that with $r_m = 0.21 \text{ mm}$ and $r = 0.8 \text{ mm}$, the "thunderstorm" curve is matched fairly well. Since there are no basic differences between the three curves we will from here on use only the single-drop approach.

The pressure scale for evaporation π_E as defined by Eq. (3.49) was calculated for several points on the curves of Fig. 3.5 and 3.6 for $r = 0.5, 0.8$ and 1.0 mm by the constant mass flux and constant divergence methods. The variation of π_E with pressure may be seen in Figs. 3.7 and 3.8, which also show the variation of $\Delta\chi$ with pressure. Although π_E varies linearly with pressure for both methods, in the constant mass flux it increases with pressure and shows a variation of 8 mb while in the constant divergence it decreases with pressure showing a variation of 70 mb, this stronger variation being explained by the term ρw which, in this case, is linear with pressure and appears in the numerator in the definition of π_E (Eq. 3.49 or 3.50). The behavior of $\Delta\chi$ is also a little different in the two methods but this may provide a way to decide which of the methods is more realistic by comparing the computed profiles to the actual profile of $\Delta\chi$ in a downdraft current.

The behavior of π_E may be described by the relationship

$$\pi_E = \pi_E(p_I) [1 + \alpha (p - p_I)]. \quad (3.53)$$

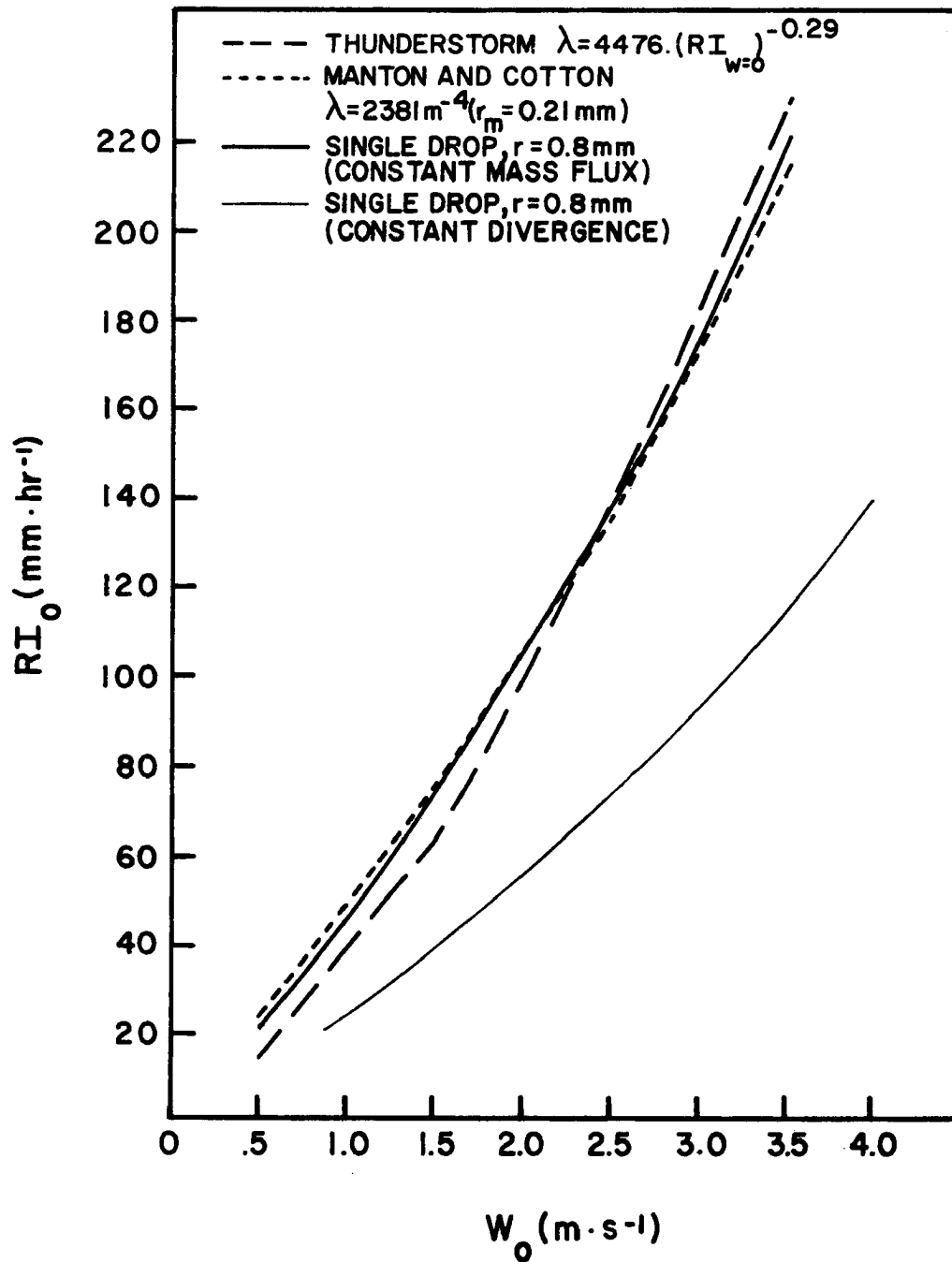


Figure 3.6. Initial rainfall intensities and downdraft speeds for different drop distributions using as reference the "thunderstorm" curve of Figure 3.5.

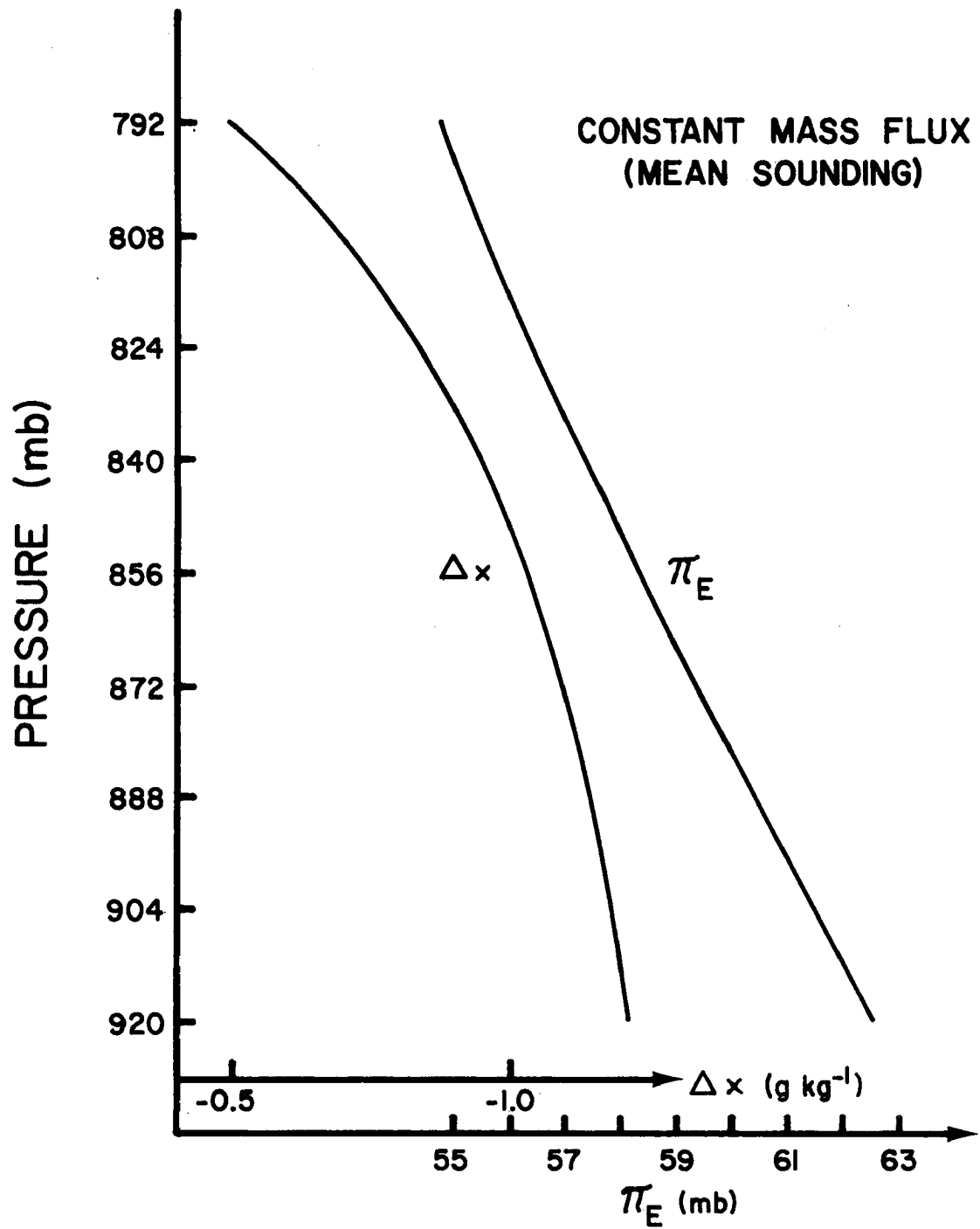


Figure 3.7. Variation of Δx and π_E for the constant mass flux case.

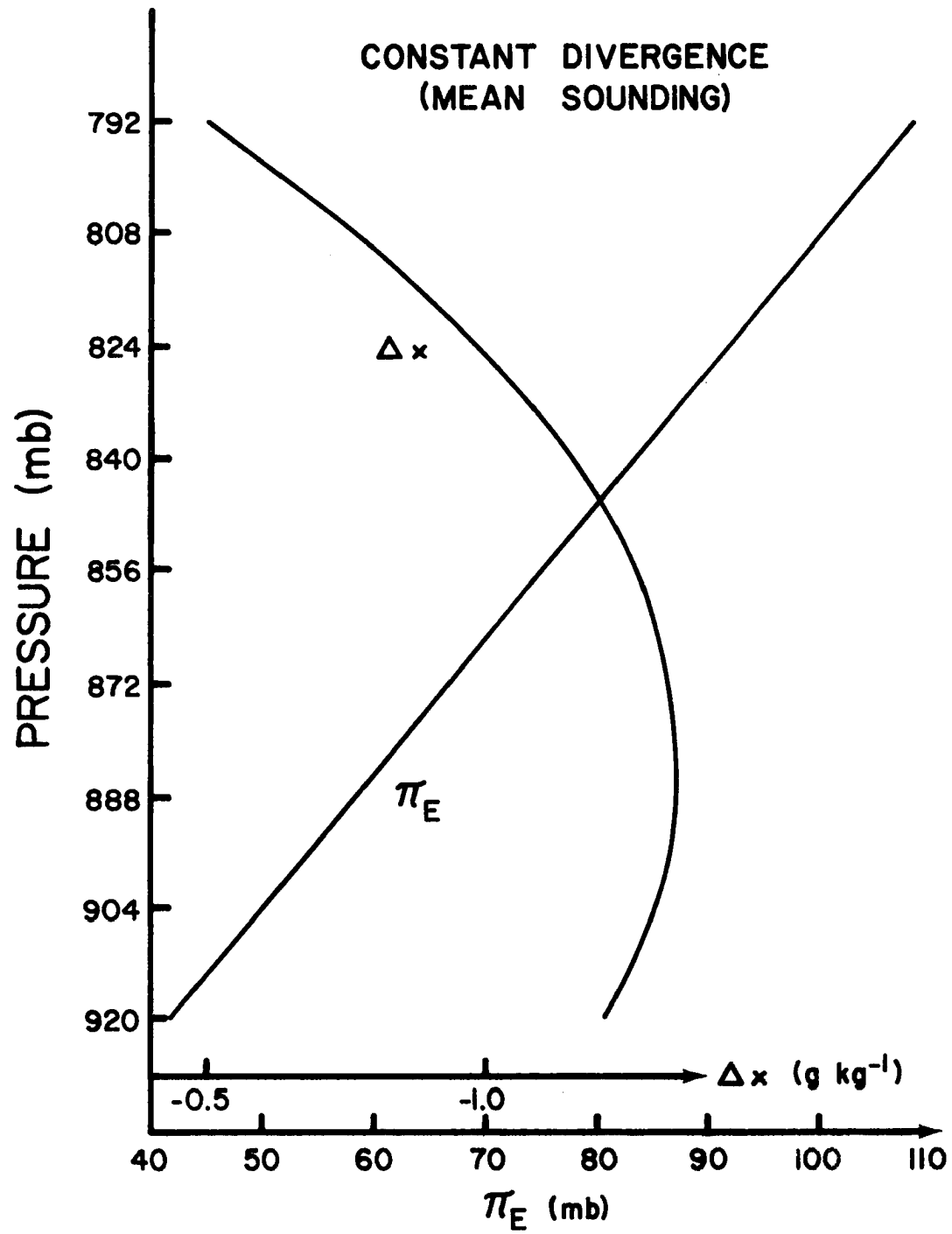


Figure 3.8. Same as Figure 3.7 for the constant divergence case.

Eq. (3.53) was fitted to the computed values of π_E and the values of $\pi_E(p_I)$ and α obtained for $r_0 = 0.5, 0.8$ and 1.0 mm for some pairs of conditions expressed in Fig. 3.5 and 3.6 are shown in Tables 5 and 6. The variation of $\pi_E(p_I)$ and α from case to case may be due to the fact that the matching of the "after" condition of Table 3 is not exact. In the constant mass flux case the mean value of $\pi_E(p_I)$ is 55.3 mb and of α , $0.15 \times 10^{-2} \text{ ms}^{-1}$. In the constant divergence case the mean $\pi_E(p_I)$ is equal to 108.8 mb and the mean α , $0.48 \times 10^{-2} \text{ mb}^{-1}$. The low variability of these parameters suggests that it is sufficient to calculate them for only one condition by fixing, for example, the rainfall intensity and the drop radius as $100 \text{ mm} \cdot \text{hr}^{-1}$ and 0.8 mm respectively, and allowing the downdraft speed to vary in order to match the desired conditions. This will be done in the next section when we look at the individual soundings.

Since the maximum rainfall intensities recorded during VIMHEX-72 corresponding to 5 min values are below $150 \text{ mm} \cdot \text{hr}^{-1}$ we may infer from Fig. 3.6 that the downdraft speeds are bound to be less than $4 \text{ m} \cdot \text{s}^{-1}$, otherwise the rainfall intensities get too high. This value is perhaps low for mid-latitude storms but seems to be adequate in the tropics.

3.3.2 Results for all soundings

The values of $\pi_E(p_I)$ and α were shown to be quite independent of the conditions in $(RI, w, r)_0$ so that we may fix two of these variables, e.g. the rainfall intensity and the drop size, and determine w_0 and consequently, $\pi_E(p_I)$ for all pairs of soundings whose end conditions are shown in Table 3. The rainfall intensity was fixed at $100 \text{ mm} \cdot \text{hr}^{-1}$ and the drop radius at 0.8 mm. The calculated w_0 , $\pi_E(p_I)$ and α for the

Constant mass flux									
$r_o = 0.5 \text{ mm}$				$r_o = 0.8 \text{ mm}$			$r_o = 1.0 \text{ mm}$		
w_o	RI	$\pi_E(p_I)$	α	RI	$\pi_E(p_I)$	α	RI	$\pi_E(p_o)$	α
m.s^{-1}	mm.hr^{-1}	mb	$\text{mb}^{-1} \times 10^{-2}$	mm.hr^{-1}	mb	$\text{mb}^{-1} \times 10^{-2}$	mm.hr^{-1}	mb	$\text{mb}^{-1} \times 10^{-2}$
0.5	8.5	54.9	0.25	21.0	55.1	0.14	30.0	58.0	0.13
1.0	18.5	56.0	0.22	46.0	54.3	0.13	68.0	54.9	0.12
1.5	31.0	55.0	0.19	74.0	54.4	0.12	106.5	55.8	0.11
2.0	44.5	55.9	0.18	105.0	54.7	0.11			
2.5	60.0	56.1	0.16	140.0	54.6	0.11			
3.0	78.0	55.8	0.15	179.0	54.4	0.10			
mean $\pi_E(p_I) = 55.3 \text{ mb}$				$\sigma_\pi = 1.0 \text{ mb}$					
mean $\alpha = 0.15 \times 10^{-2} \text{ mb}^{-1}$				$\sigma_\alpha = 0.04 \times 10^{-2} \text{ mb}^{-1}$					

Table 5. Variation of the parameters $\pi_E(p_I)$ and α in the constant mass flux case for different values of drop radii, downdraft speeds and rainfall intensities.

Constant Divergence											
$r_o = 0.5 \text{ mm}$				$r_o = 0.8 \text{ mm}$				$r_o = 1.0 \text{ mm}$			
w_o	RI_o	$\pi_E (p_I)$	α	w_o	RI_o	$\pi_E (p_I)$	α	w_o	RI_o	$\pi_E (p_o)$	α
m.s^{-1}	mm.hr^{-1}	mb	mb^{-1}	m.s^{-1}	mm.hr^{-1}	mb	mb^{-1}	m.s^{-1}	mm.hr^{-1}	mb	mb^{-1}
			$\times 10^{-2}$				$\times 10^{-2}$				$\times 10^{-2}$
0.7	8.5	*100.6	-0.46	0.9	21.0	110.5	-0.48	0.9	30.0	110.7	-0.48
1.5	18.5	104.7	-0.46	1.7	46.0	108.8	-0.48	1.8	68.0	110.3	-0.48
2.2	31.0	104.8	-0.49	2.5	74.0	108.3	-0.48	2.5	107.0	109.4	-0.48
3.0	44.5	108.6	-0.47	3.3	105.0	109.4	-0.48				
3.7	60.0	109.2	-0.47	4.0	140.0	109.3	-0.48				
4.4	78.0	108.0	-0.47	4.9	179.0	111.4	-0.48				

mean $\pi_E (p_I) = 108.8 \text{ mb}$

$\sigma_\pi = 2.0 \text{ mb}$

mean $\alpha = 0.48 \times 10^{-2} \text{ mb}^{-1}$

$\sigma_\alpha = 0.01 \times 10^{-2} \text{ mb}^{-1}$

(excluding *)

Table 6. Same as Table 5, for the constant divergence case.

constant mass flux case and w_0 , Div , $\pi_E(p_I)$ and α for the constant divergence case may be seen in Table 7. It may be seen that the downdraft speeds change considerably from case to case as does $\pi_E(p_I)$. In the cases where there are two or three "after" soundings, the downdraft speeds obtained vary a lot. For example, soundings 100-101 give a $1 \text{ m}\cdot\text{s}^{-1}$ downdraft speed in the 'constant mass flux' case (or $1.8 \text{ m}\cdot\text{s}^{-1}$ in the 'constant divergence' case) and soundings 100-102 give a $2.4 \text{ m}\cdot\text{s}^{-1}$ downdraft speed in the constant mass flux case (or $3.6 \text{ m}\cdot\text{s}^{-1}$ in the constant divergence case). This shows that either the different "after" soundings express the properties of air coming from different levels in the atmosphere and in that case, the different downdraft speeds are representative of different stages in the life cycle of the storm or the different downdraft speeds would be an indication of the sensitivity of the method to the different initial conditions.

Table 7 also shows that α , as computed by the constant mass flux method, is remarkably constant so that in this case we are left with only one parameter which specifies the microphysical processes. In the constant divergence case, the variation of α is a little bit higher but with the exclusion of the value of soundings 120-122 which appear to be anomalous, we may forget about this variability and consider $\pi_E(p_I)$ as the only parameter that needs to be specified.

In the next chapter the relationship between $\pi_E(p_I)$ and pre-storm parameters and its potential as a model parameter will be investigated.

3.3.3 Results for constant θ_E soundings

The soundings which represented a deep layer of reasonably constant θ_E were 82, 317, 3.25. The initial level where we started the

Sounding no.	Constant Mass flux			Constant divergence			Div s ⁻¹
	w_0 m.s ⁻¹	$\pi_E(p_I)$ mb	α mb ⁻¹ x10 ⁻²	w_0 m.s ⁻¹	$\pi_E(p_I)$ mb	α mb ⁻¹ x10 ⁻²	
59-60	1.1	31.3	0.10	1.70	54.0	-0.72	1.25 x10 ⁻³
59-61	0.8	22.3	0.10	1.25	38.2	-0.81	1.05
81-82	2.6	71.6	0.13	4.38	154.0	-0.36	1.50
81-83	2.4	62.7	0.12	4.10	135.9	-0.34	1.30
100-101	1.0	25.7	0.11	1.80	54.2	-0.54	0.95
100-102	2.4	69.6	0.13	3.59	125.2	-0.42	1.45
116-117	2.3	72.8	0.12	3.60	136.7	-0.58	2.10
120-121	1.4	34.9	0.12	2.11	61.6	-0.42	0.85
120-122	0.7	21.1	0.12	0.96	30.5	-1.64*	1.70
120-123	1.8	53.0	0.11	2.66	90.5	-0.58	1.55
131-132	2.1	70.4	0.10	3.10	119.1	-0.81	2.60
131-133	2.1	66.7	0.11	3.15	116.2	-0.64	2.05
176-177	0.7	14.9	0.11	1.66	43.7	-0.37	0.57
176-178	1.1	31.9	0.12	1.73	56.5	-0.81	1.45
192-193	1.7	47.2	0.11	2.60	84.7	-0.49	1.25
192-194	1.3	38.0	0.10	1.90	62.1	-0.72	1.40
203-204	2.1	58.5	0.13	3.48	119.4	-0.42	1.90
226-228	1.9	59.1	0.12	2.91	105.7	-0.64	1.50
241-242	2.7	75.6	0.13	4.38	154.3	-0.36	1.05
241-243	1.9	48.2	0.12	3.06	94.8	-0.37	0.60
312-317	0.7	15.3	0.11	1.61	43.4	-0.40	1.10
312-318	2.1	51.2	0.13	3.71	116.7	-0.32	0.60
324-325	1.1	25.0	0.11	1.74	46.6	-0.37	2.80
324-326	2.9	101.8	0.10	4.30	178.7	-0.64	2.80
Mean Sounding	1.9	54.7	0.11	3.17	109.4	-0.48	1.50

$$\begin{aligned}\text{mean } \pi_E(p_I) &= 48.7 \text{ mb} \\ \text{mean } \alpha &= 0.12 \text{ mb}^{-1} \\ \sigma_{\pi} &= 22.8 \text{ mb} \\ \sigma_{\alpha} &= 0.01 \text{ mb}^{-1}\end{aligned}$$

$$\begin{aligned}\text{mean } \pi_E(p_I) &= 94.3 \text{ mb} \\ \text{mean } \alpha &= 0.53 \text{ mb}^{-1} \text{ (exclude *)} \\ \sigma_{\pi} &= 43.2 \text{ mb} \\ \sigma_{\alpha} &= 0.17 \text{ mb}^{-1}\end{aligned}$$

In all cases $RI_0 = 100 \text{ mm.hr}^{-1}$, $r_0 = 0.8 \text{ mm}$ (the result shown is independent of this choice as discussed in the text).

Table 7. Parameters $\pi_E(p_I)$ and α for all soundings.

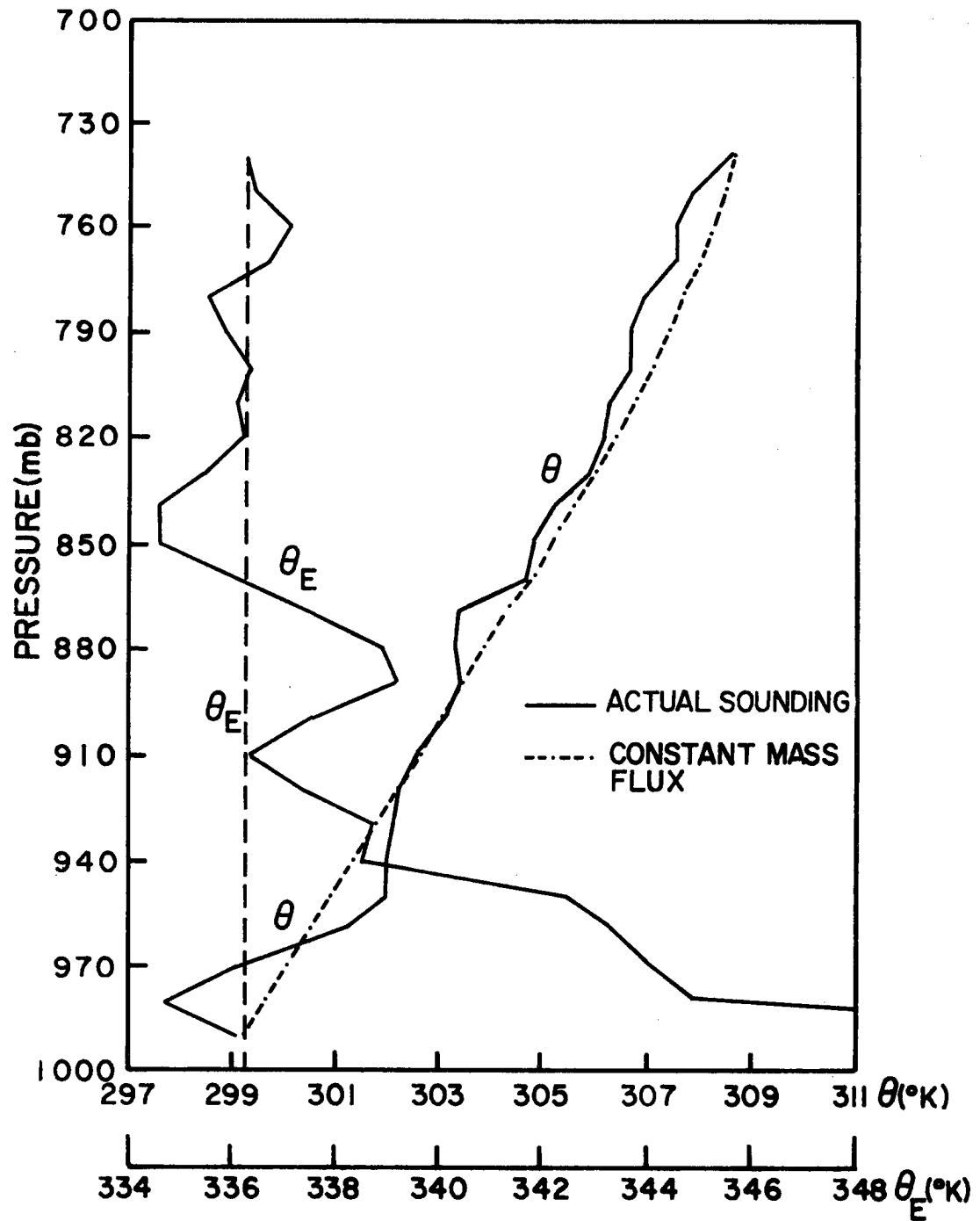


Figure 3.9. Potential temperature and equivalent potential temperature in sounding 82 and as calculated using the constant mass flux approach.

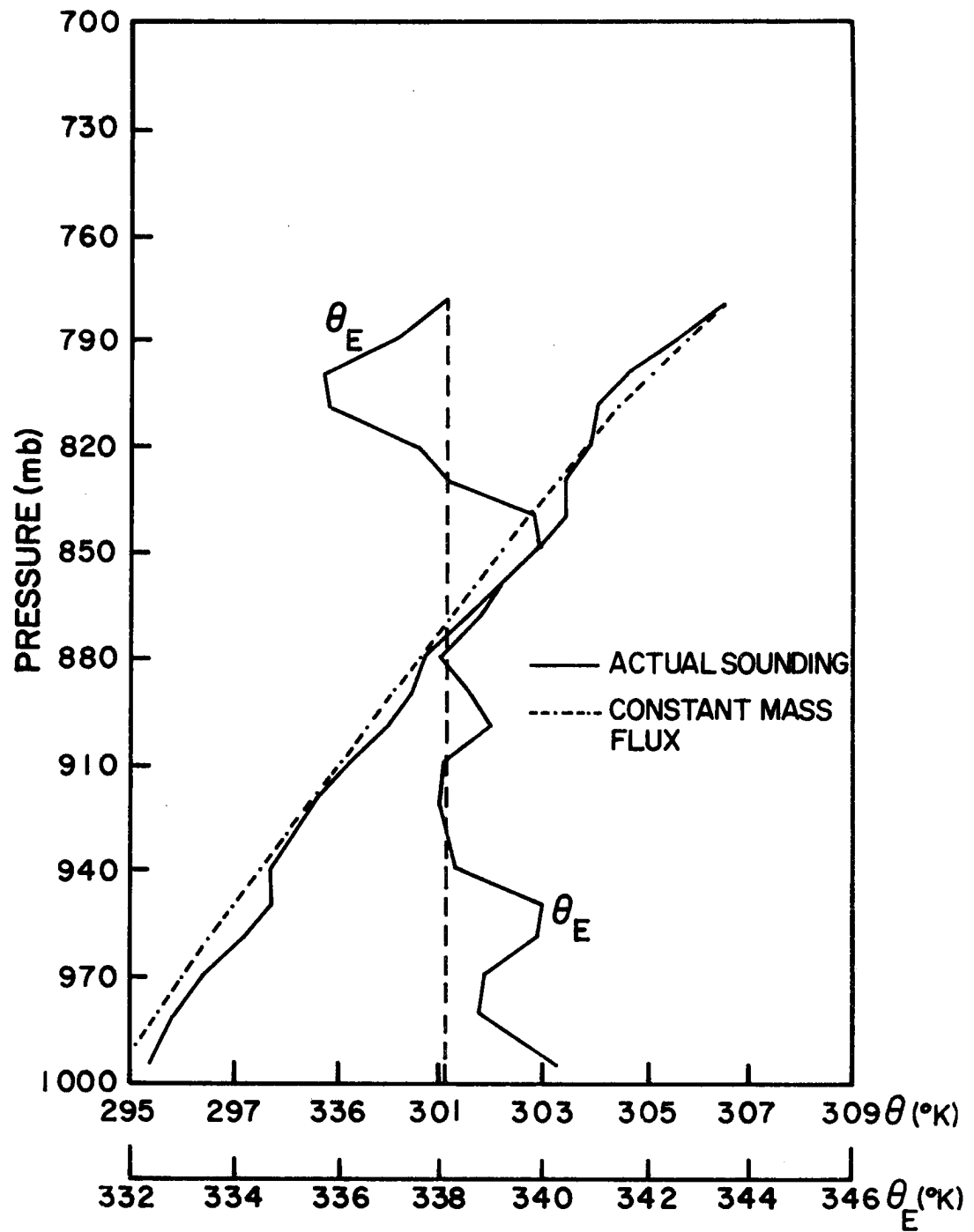


Figure 3.10. Same as Figure 3.9, for sounding 317.

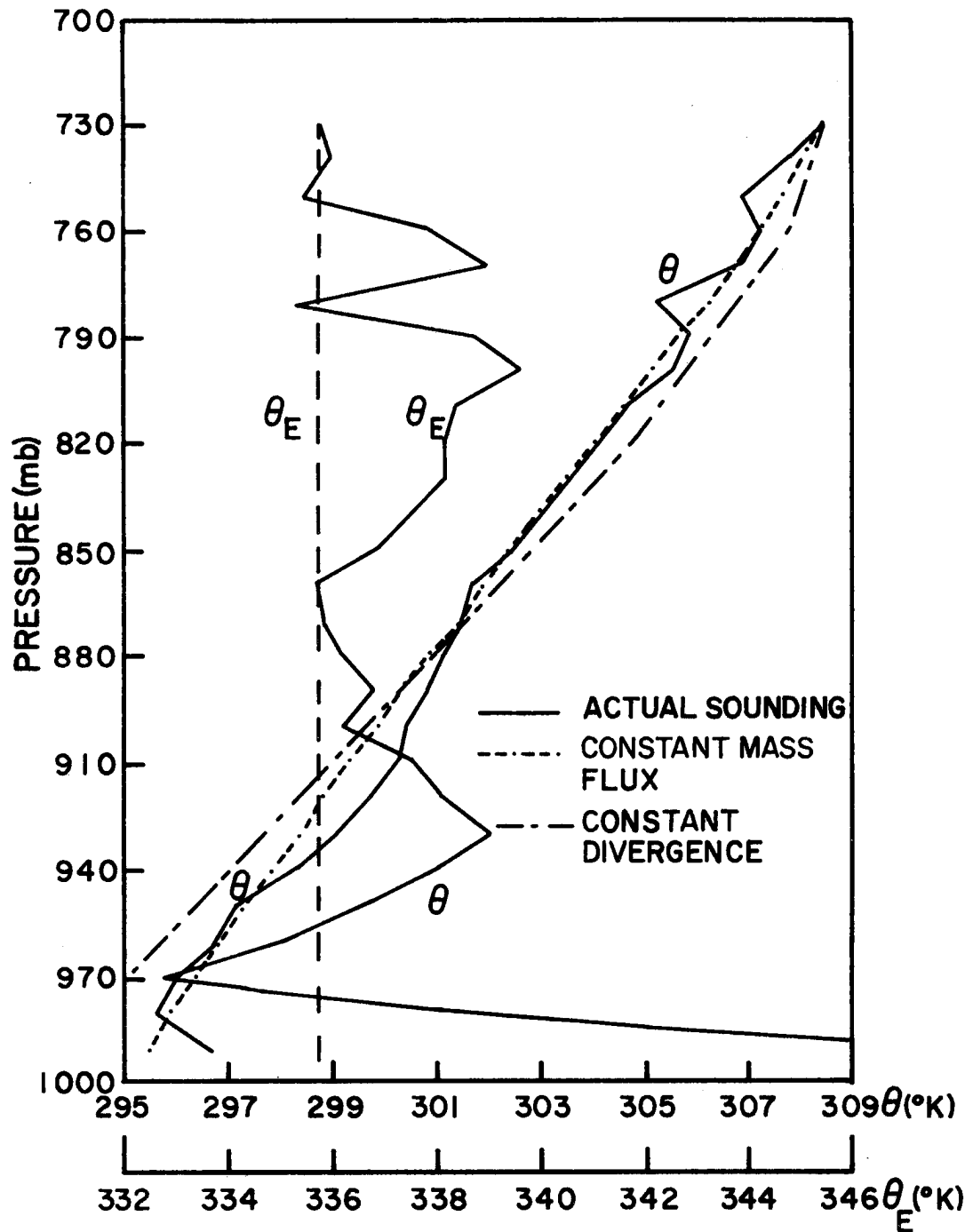
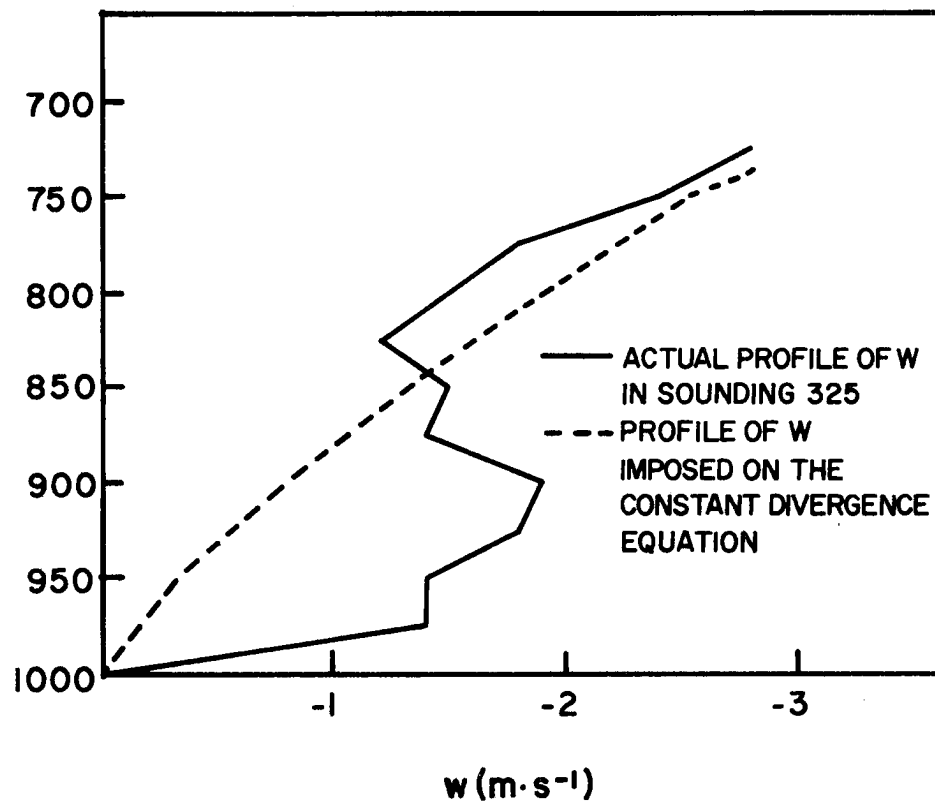


Figure 3.11. Same as Figure 3.10, for sounding 325. The profile of potential temperature from the constant divergence approach is also shown.



3.12. Deviation of the rawinsonde from a constant rate of ascent during sounding 325 and profile of vertical velocity imposed on the constant divergence approach.

computations may be seen in Table 4. These soundings showed a layer close to the surface where θ_E increased considerably. This is related to the increase in moisture close to the surface since θ_E is very sensitive to variations in water vapor mixing ratio. The profiles of θ and θ_E for the three mentioned soundings may be seen in Figs. (3.9), (3.10) and (3.11), for the constant mass flux case. The profiles of θ obtained show a smoothed version of the actual profile. Sounding 325 is a particularly interesting one since the rawinsonde got into the downdraft air. The deviation of the balloon from a constant rate of ascent may be seen in Fig. (3.12). In that case, the constant divergence method was applied with a profile of w which is also shown in Fig. (3.12). The drop radius was fixed at 0.8 mm. The profile of θ obtained may be seen in Fig. 3.11. In order to obtain this profile, an initial rainfall intensity of $160 \text{ mm}\cdot\text{hr}^{-1}$ was required, which reached the ground level as $93 \text{ mm}\cdot\text{hr}^{-1}$. The maximum rainfall intensity associated with this storm was $61 \text{ mm}\cdot\text{hr}^{-1}$ as given in Table 8. This difference is not significant due to the variability of rainfall data from one station to another, and to the fact that the maximum rainfall intensity related to the system may not have occurred over a recording rainguage.

This result shows that the method used is close enough to what is going on in the atmosphere, however, due to the lack of enough soundings launched under the conditions of sounding 325, this conclusion cannot be checked further.

Fig. 3.11 shows the the θ -profile is more accurately reproduced with the constant mass flux approach suggesting that perhaps the divergence of the downdraft air occurs in a shallower layer than the one assumed in Fig. 3.12.

Date, Sound Time Station	June 19 (59-61) 1419-1654		June 27 (81-83) 1806-2126		July 3(100-102) 1956-2222		July 8(116-117) 1801-2003	
	Total	Max.R.I.	Total	Max.R.I.	Total	Max.R.I.	Total	Max.R.I.
WG 1	3.5	42.0	0.5	6.0	2.3	6.0	6.8	49.2
WG 4	0.5	6.0	6.4	25.2	3.6	18.0	1.5	5.2
WG 7	4.6	27.6	6.8	30.0	---	---	---	---
WG 9	---	---	6.8	27.6	1.8	15.6	1.0	3.6
WG10	0.5	3.6	3.8	18.0	---	---	---	---
FA 1	15.3	8.4	1.2	4.8	5.5	33.6	---	---
FA 6	5.6	21.6	16.8	50.4	5.8	46.8	---	---
Mean	4.3	26.4	6.0	23.1	2.7	17.1	1.3	8.3
Max.	15.3	84.0	16.8	50.4	5.8	46.8	6.8	49.2
	July 9(120-123) 1523-1936		July 11(131-133) 1253-1627		July 24(176-178) 1713-1934		July 28(192-194) 1843-2125	
WG 1	11.50	31.80	---	---	2.3	12.0	18.8	106.8
WG 4	36.8	80.4	9.7	55.2	11.7	55.2	13.0	45.6
WG 7	50.5	138.0	2.0	15.6	5.1	15.6	8.9	24.0
WG 9	31.8	76.8	0.8	4.8	1.0	3.6	4.6	9.6
WG10	6.9	31.2	23.1	106.8	15.7	43.2	---	---
FA 1	10.3	32.4	1.5	9.6	10.2	28.8	4.7	24.0
FA 6	14.5	56.4	1.8	20.4	1.2	3.6	19.2	50.4
Mean	23.2	63.9	5.6	30.3	6.7	23.1	9.9	37.2
Max.	50.5	138.0	23.1	106.8	12.2	55.2	19.2	106.8
	July 31(203-204) 1503-1845		Aug. 7 (226-228) 1759-2028		Aug. 11(241-243) 1446-1713		Sept. 1-2(312-318) 1833-1151	
WG 1	---	---	6.9	27.6	---	---	62.2	105.6
WG 4	5.6	43.2	0.2	0.2	6.4	25.2	68.3	85.2
WG 7	---	---	---	---	1.5	3.6	67.3	58.8
WG 9	---	---	---	---	15.2	118.8	61.3	50.8
WG10	---	---	---	---	1.0	6.0	136.4	81.6
FA 1	1.3	8.4	0.6	0.3	1.4	21.6	37.7	50.4
FA 6	1.5	16.8	---	---	24.4	99.6	51.1	75.6
Mean	2.8	9.8	1.1	4.0	7.1	39.3	64.9	72.6
Max.	5.6	43.2	6.9	27.6	24.4	118.8	136.4	105.6
	Sept. 4(324-326) 1522-1756							
WG 1	13.3	45.6						
WG 4	19.1	49.2						
WG 7	15.2	37.2						
WG 9	5.6	31.2						
WG10	9.4	61.2						
FA 1	1.0	7.2						
FA 6	11.8	40.8						
Mean	10.8	38.9						
Max.	19.1	61.2						

Table 8. Total rainfall and maximum rainfall intensity at seven stations located within 20 km from Carrizal in the time intervals between soundings.

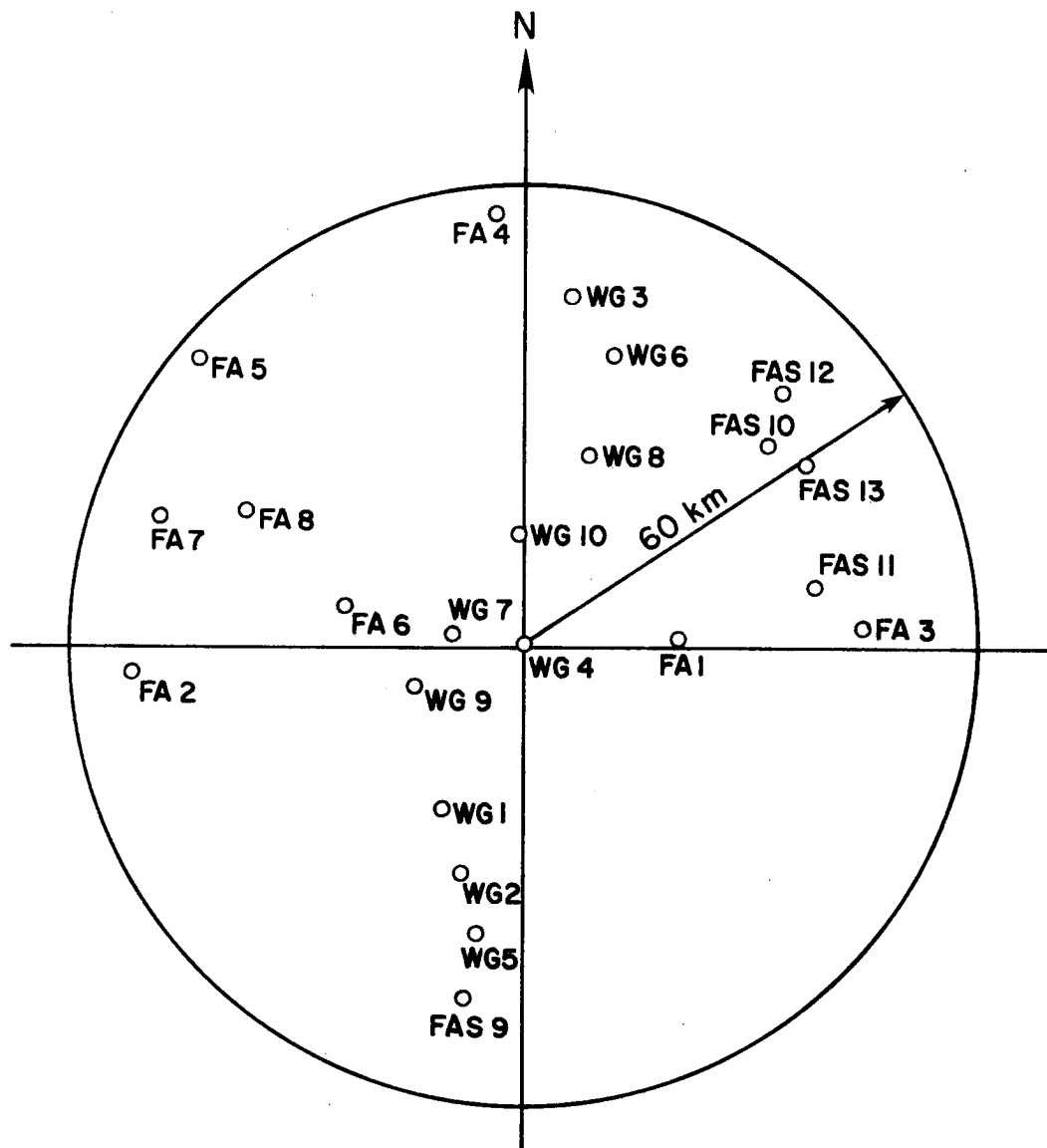
The next sections will only be concerned with the results corresponding to Betts (1976) model, but it should be noted that the constant θ_E soundings are a particular case of Betts (1976) model: one in which the rawinsonde is always inside the downdraft air so that it is measuring the properties of the air in the descending layer (Fig. 1.1 or 3.3).

3.3.4 Comparison with data

In this section we will present the available rainfall data and downdraft speed magnitudes in order to compare them with the results of section 3.3.2. In VIMHEX-72 there were no measurements of raindrop sizes. The only estimate we have for the downdraft speed is the deviation of the balloon from a constant rate of ascent and so, only those soundings which got into the downdraft air may present some significant value. Even in the cases where it is possible to estimate a downdraft speed profile, it should be noted that the balloon will not ascend under downdraft speeds bigger than $4 \text{ m}\cdot\text{s}^{-1}$, so that we will be underestimating the maximum downdraft speed reached in a given system. Table 9 shows the cases in which the downdraft would have some meaning, i.e., when the maximum deviation of the balloon speed from the constant rate of ascent is bigger than $1 \text{ m}\cdot\text{s}^{-1}$. The rainfall data in VIMHEX-72 were taken at several ground stations; the recording raingauges are shown in Fig. 3.13. They are all inside a circle of 60 km centered at Carrizal. The data used here are of those stations inside a circle of radius 20 km centered at Carrizal. The values of total rain in millimeters and maximum rainfall intensities in millimeters per hour, for the seven stations considered and for each storm system, may be seen in Table 8.

Sound. no.	Maximum observed w from rawinsonde data (m, s^{-1})	Maximum RI from Table 8 (mm, hr^{-1})	Value of w corresponding to observed max RI + 50% using μ_0 (const. Div) from Table 7 ($r = 0.8$ mm)
59 - 60	1.2	84.0	2.1
59 - 61			1.5
100 - 101	2.2	46.8	1.4
100 - 102			2.9
116 - 117	1.2	49.2	2.9
120 - 121			3.8
120 - 122	1.6	138.0	1.8
120 - 123			4.6
131 - 132	1.8	106.8	4.4
131 - 133			4.5
176 - 177	1.9	55.2	1.5
176 - 178			1.5
203 - 204	2.1	43.2	2.6
312 - 317	1.6	105.6	2.5
312 - 318			5.3
324 - 325	2.8	61.2	1.7
324 - 326			4.1

Table 9. Comparison of the downdraft speed as calculated using the parameters of Table 7 with the maximum observed deviation of the rawinsonde from a constant rate of ascent.



3.13 Locations of recording rain gauges. WG4 is located at Carrizal, Venezuela ($9^{\circ} 22.8'N$, $66^{\circ} 55.0'W$).

Single drop		Constant mass flux		Constant divergence	
r_{top}	RI_{top}	RI_{top}	r_{top}	RI_{top}	r_{top}
(mm)	(mm.hr ⁻¹)	RI bottom	r bottom	RI bottom	r bottom
0.5	8.5	1.73	1.20	1.89	1.20
	18.5	1.64	1.18	1.95	1.18
	31.0	1.54	1.16	2.00	1.16
	44.5	1.48	1.14	2.05	1.15
	60.0	1.44	1.13	2.08	1.14
	78.0	1.39	1.12	2.11	1.13
0.8	21.0	1.21	1.07	1.35	1.08
	46.0	1.19	1.06	1.43	1.07
	74.0	1.18	1.06	1.49	1.06
	105.0	1.17	1.05	1.55	1.06
	140.0	1.16	1.05	1.60	1.06
	179.0	1.14	1.05	1.65	1.05
1.0	30.0	1.14	1.04	1.24	1.05
	68.0	1.12	1.04	1.32	1.04
	107.0	1.12	1.04	1.38	1.04

Drop spectrum, constant mass flux
Manton and Cotton parameters

$$r_m = 0.21 \text{ mm } (\lambda = 2381 \text{ m}^{-1})$$

n_o	RI_{top}	RI_{top}	$n_o \text{ top}$
m ⁻³	(mm.hr ⁻¹)	RI bottom	n_o bottom

Kessler parameters (thunderstorm)

$$n_o = 1.6 \times 10^7 \text{ m}^{-3}$$

λ	RI_{top}	RI_{top}	$\lambda \text{ top}$
(m ⁻¹)	(mm.hr ⁻¹)	RI bottom	λ bottom

2.2X10 ⁸	25.0	1.19	1.11	2143.	14.0	1.37	0.92
4.9	65.0	1.19	1.11	1432.	64.0	1.21	0.95
5.6	75.0	1.18	1.09	1188.	136.0	1.16	0.97
13.1	220.0	1.14	1.05	1048.	230.0	1.13	0.98

Table 10. Ratio between rainfall intensities, drop radius or drop distribution parameters at the top and at the bottom of the layer for different initial conditions.

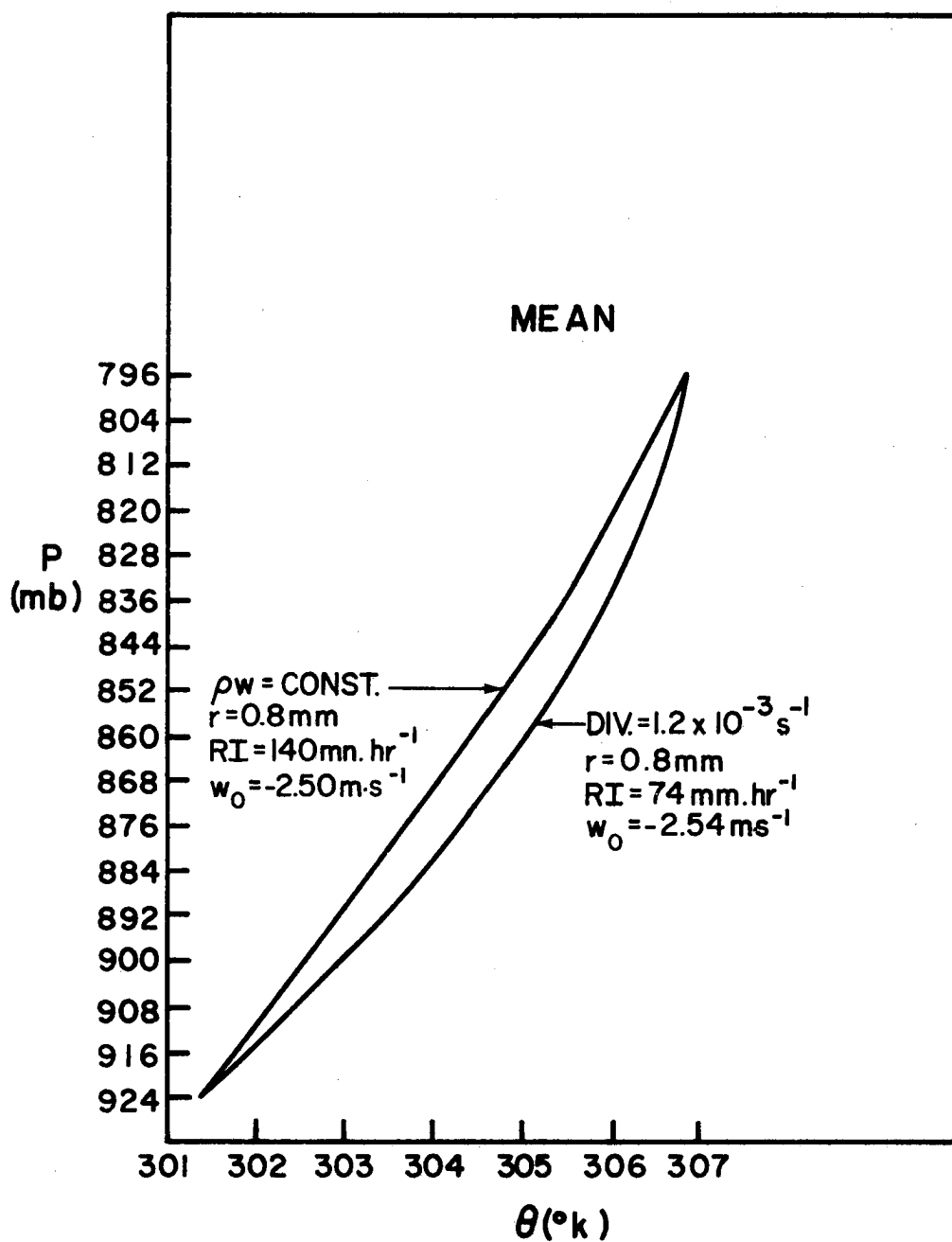


Figure 3.14. Vertical profile of potential temperature obtained using the constant mass flux and constant divergence approaches, using the mean "before" and "after" conditions.

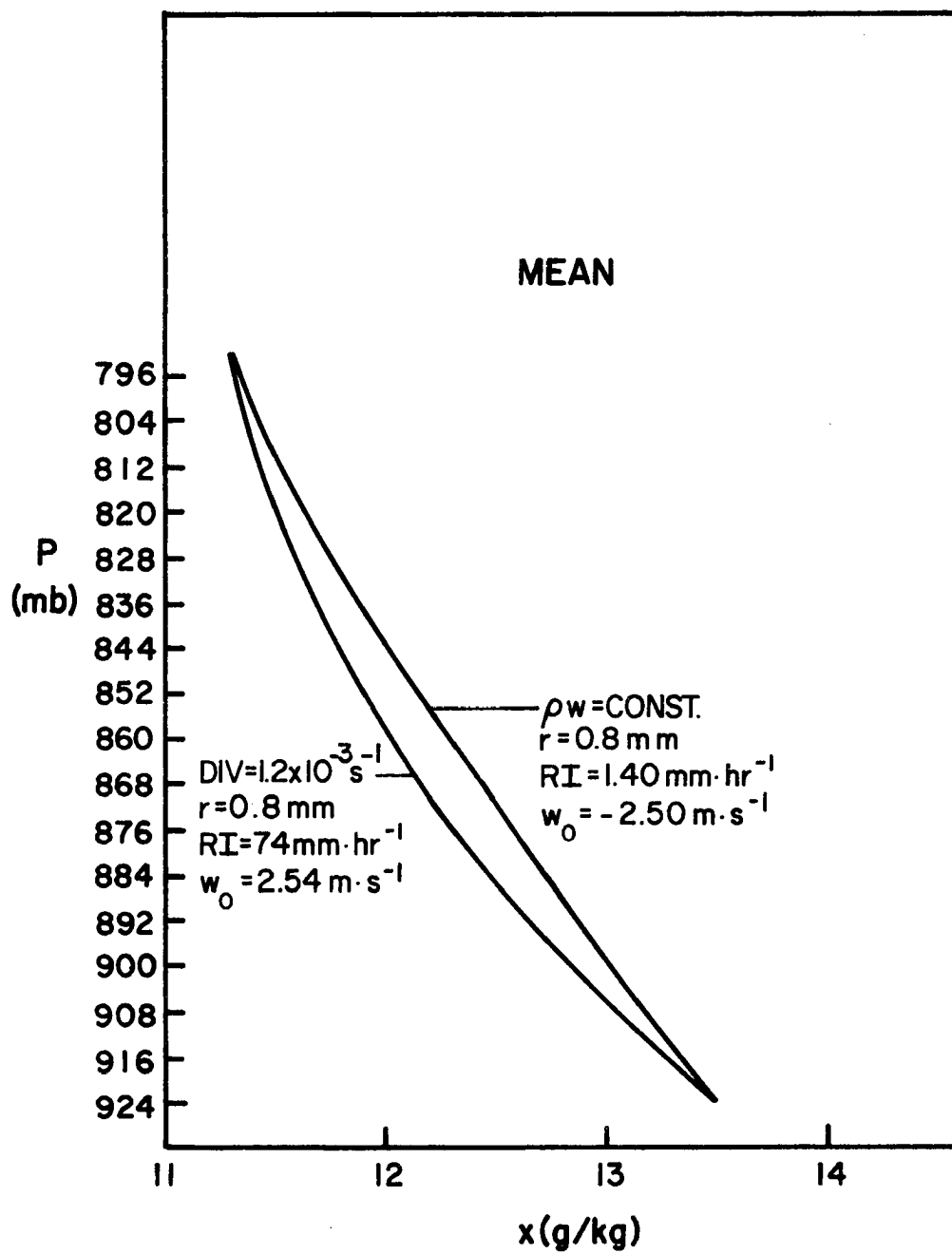


Figure 3.15. Vertical profile of mixing ratio obtained using the constant mass flux and constant divergence approaches, using the mean "before" and "after" conditions.

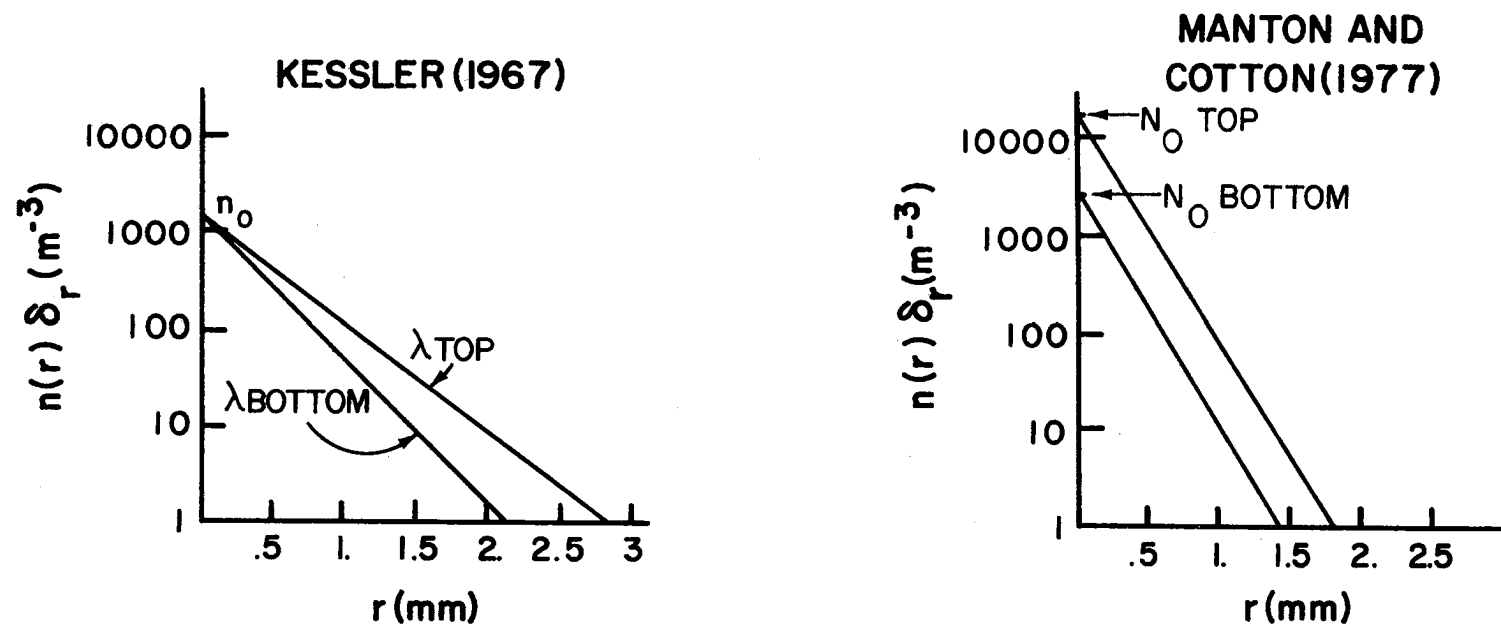


Figure 3.16. Drop spectrum variation with height for the Manton and Cotton (1977) and Kessler (1969) parameterizations.

The scattering of the data is related to the travel path of the system. The maximum rainfall intensity within the seven stations is listed again in Table 9 for each storm. We may now compute the downdraft speeds that should correspond to these rainfall intensities. To do this, we consider that the rainfall intensities observed are ground values so that we may account for the evaporation that has been taking place and add 50% to the ground values in order to obtain a rainfall intensity higher up in the atmosphere. Then, by the use of the calculated value of μ_0 , for the constant divergence case, and assuming a drop radius of 0.8 mm, we may compute w (using Eq. 3.50, 3.28 and 3.15).

The downdraft speed computed in this way may be seen in the third column of Table 9. As may be seen, the different pairs of soundings related to the same system give different downdraft speeds but this may also be related to different stages of the system. It should also be noted that the different storms are probably associated with different drop spectra and this would influence the calculated downdraft speeds. Anyway, the calculated downdraft speeds seem to be reasonable considering the unrepresentativeness of the magnitude of the downdraft speeds obtained from rawinsonde data.

3.4 Vertical variation of some calculated variables

Until now, only the profile of mixing ratio has been presented, given by the parameters μ_0 and α of Table 7. In this section, the variation with height of potential temperature, rainfall intensity and drop radius will be briefly presented and discussed for the constant mass flux and for the constant divergence cases with some considerations about the different results with the single-drop and drop spectrum equations.

3.4.1 Profile of potential temperature

The profile of θ obtained with the single-drop and the drop spectrum equations is the same, but comparing the constant mass flux and the constant divergence profiles as in Fig. 3.14 we see that the slopes are different. In the constant mass flux case the slope is almost constant while in the constant divergence the slope is a function of height. This kind of variation is also observed in the mixing ratio as may be seen in Fig. 3.15. This difference is associated with the strong variation with height of the downdraft speed in the constant divergence case. Computing the slope of potential temperature in the constant mass flux case for all soundings, it is found that it does not change very much from one pair of soundings to another, the mean being $5.0^{\circ}\text{K}/100\text{ mb}$ with a standard deviation of $1.6^{\circ}\text{K}/100\text{ mb}$.

The profile of θ found in downdrafts may present an indication of whether the ρ_w profile is constant or linear with height, i.e. whether the divergence of the downdraft air occurs in a shallow layer near the surface or in a deeper layer as required by the constant divergence approach.

3.4.2 Depletion of rainfall intensities and drop radius

The variation in the rainfall intensity and drop radius, or drop spectrum parameter with height, as may be seen in Table 10, depends on the method used. In the case of the drop spectrum, the Manton and Cotton parameterization shows that the number of small and of big drops is decreased with decreasing height while in the Kessler parameterization the number of big drops decreases with decreasing height. This may be seen in the schematic diagram in Fig. (3.16). For rainfall

intensities less than approximately $140.0 \text{ mm}\cdot\text{hr}^{-1}$, there is more evaporation going on in the Kessler parameterization than in the Manton and Cotton parameterization (Table 10), while for very high rainfall intensities the reverse is true. Manton and Cotton (1977) suggested that their parameterization requires more evaporation than Kessler's (1967) parameterization for rain densities greater than $5.97 \text{ g}\cdot\text{m}^{-3}$. In fact, for a rainfall intensity of $64 \text{ mm}\cdot\text{hr}^{-1}$ and downdraft speed of $1.5 \text{ m}\cdot\text{s}^{-1}$, the rain density according to Eq. (3.28) is approximately $2.4 \text{ g}\cdot\text{m}^{-3}$ while for a rainfall intensity of $230 \text{ mm}\cdot\text{hr}^{-1}$ with a downdraft speed of $3.5 \text{ m}\cdot\text{s}^{-1}$, the rain density is $6.4 \text{ g}\cdot\text{m}^{-3}$, showing an agreement with the Manton and Cotton (1977) computations.

In the single drop case, there is more evaporation going on in the constant divergence case than in the constant mass flux case perhaps because of the greater ventilation that is allowed to take place when there is horizontal flow of air. The decrease in the raindrop radius is the same in both cases. This is possible since the conservation equations are different.

In the constant mass flux case, the smaller the rainfall intensity, the slower the air will be descending and so there is more time for the evaporation to take place. In the constant divergence case, there will be a compromise between the slower descending air which allows more time for the evaporation process and the fact that the greater the initial downdraft speed, the greater is the decrease in rainfall intensity since w must be zero at the ground. This explains why the ratio between the rainfall intensity at the top and the bottom in the constant divergence case shows a different behavior than in the constant mass flux case.

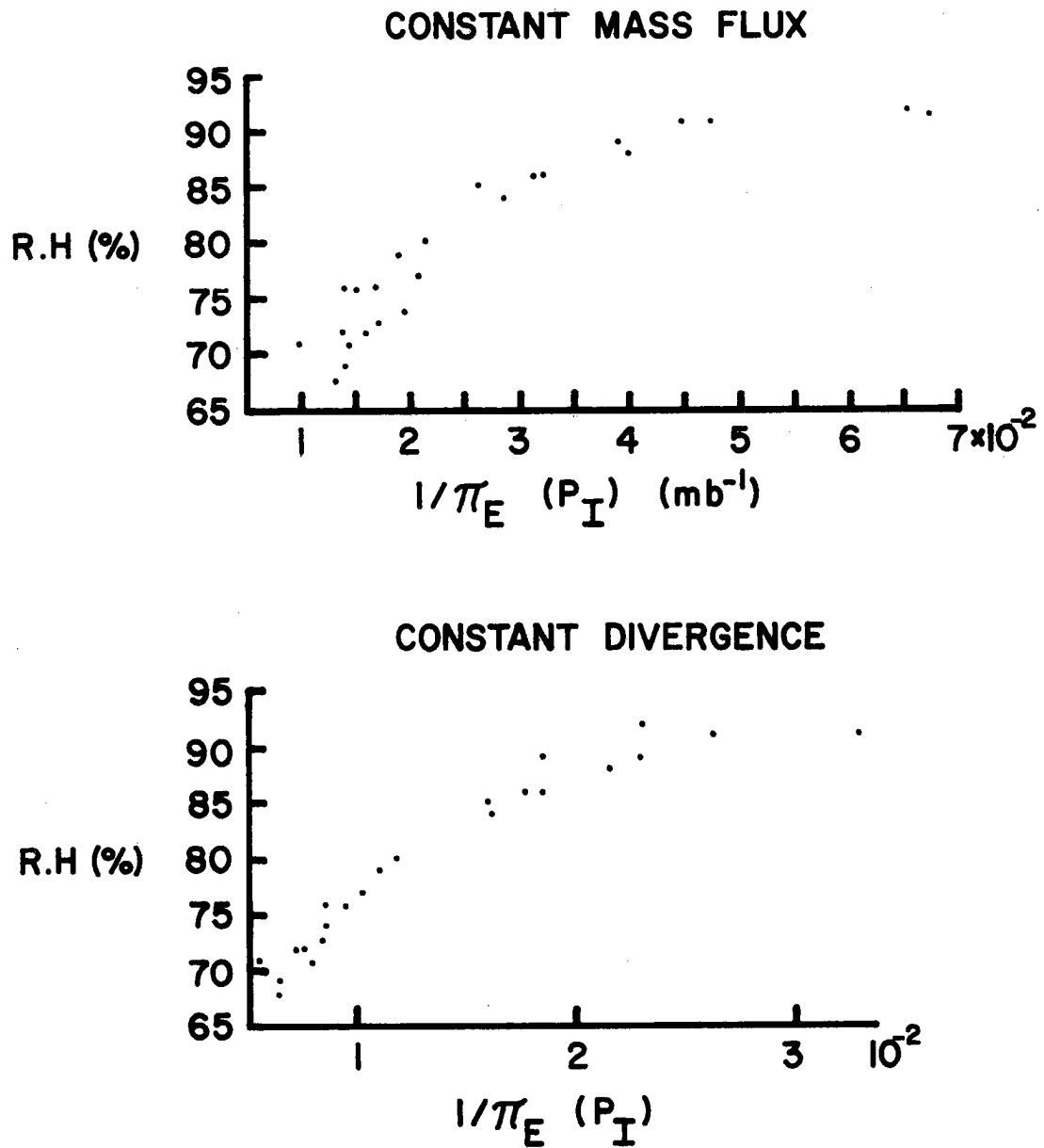


Figure 4.1. A plot of $\pi_E(p_I)^{-1}$ vs. lower layer averaged relative humidity for the constant mass flux and constant divergence approaches.

IV. MODELLING CONCLUSIONS

The purpose of this chapter is to use the diagnostic results of Chapter III in order to present some suggestions on how they may be helpful in the modelling of the downdraft structure in tropical storms. The modification of the subcloud layer temperature and moisture profiles by the downdraft associated with the passage of a raining system was shown to depend essentially on the parameter π_E and on the temperature and moisture conditions before the storm passage. Thus, it is suggested that one should try to relate π_E to pre-storm parameters in such a way that we could know it before the storm and consequently be able to forecast the subcloud layer structure after the storm. This will be done in the first section of this chapter. Some interesting conclusions related to the physical significance of π_E will be reached in the following section where the analytical solution of the evaporation equation is presented. The last section will present some suggestions for future work and a discussion of the required experimental data to test the validity of the proposed parameterization.

4.1 The parameter π_E vs. pre-storm parameters

Among the parameters available before the storm passage, the depth of the subcloud layer given by the lifting condensation level which defines Δp in Fig. 1.1, the mean relative humidity in the upper layer and the mean wind speed in the upper layer relative to the moving storm (from p_1 to p_2 in Fig. 1.1) were chosen. The value of $\pi_E(p_I)$ for a given pair of soundings is very closely related to the mean relative humidity in the lower layer after the storm passage as may be seen in Fig. 4.1 for the constant mass flux and constant divergence methods, so

that if we find a way to specify $\pi_E(p_I)$ from some pre-storm values the mean relative humidity in the sub cloud layer after the storm will follow.

The parameter $\pi_E(p_I)$ has been averaged for each system and then $\left[\pi_E(p_I)\right]^{-1}$ plotted against the depth of the subcloud layer, the mean relative humidity at the upper layer, and the mean inflow of air in the upper layer, as may be seen in Fig. 4.2, for the constant mass flux and constant divergence cases. The plot of the relative humidity in the upper layer (Fig. 4.2 b,e) does not show any kind of trend and this should be expected since the relative humidity at this layer does not vary too much between 80 and 90%. One could suggest that the depth of the subcloud layer would show some relation to π_E : a deep subcloud layer would allow more evaporation to take place. This was not verified (Fig. 4.2 a,d) mainly because the amount of evaporation will not depend on the length of the path that the drops will have to go over but the time that it will take to cover such distance. A slow descending downdraft in a shallow layer may provide as much evaporation as a fast descending downdraft in a deep layer.

From the three variables investigated the one that has more potential to be related to the variation of π_E is the relative in-flow into the system: the stronger the in-flow the faster might be the downdraft speed according to the model in Fig. 1.1 and consequently, the greater the parameter π_E which is directly proportional to w . Fig. 4.2 c,f shows a plot of the component of the relative wind along the storm motion against $1/\pi_E$. Although there is a considerable amount of scattering there is a possibility that the expected relationship would hold if more data were used.

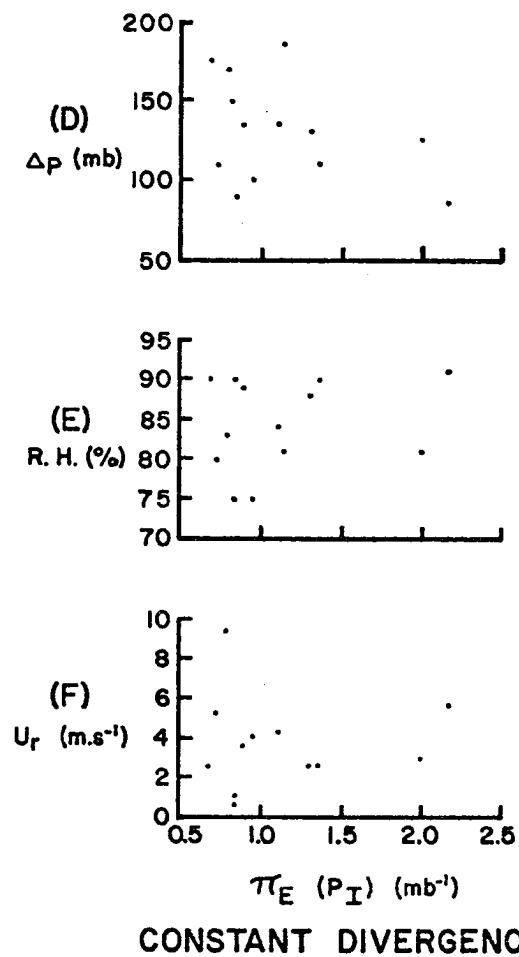
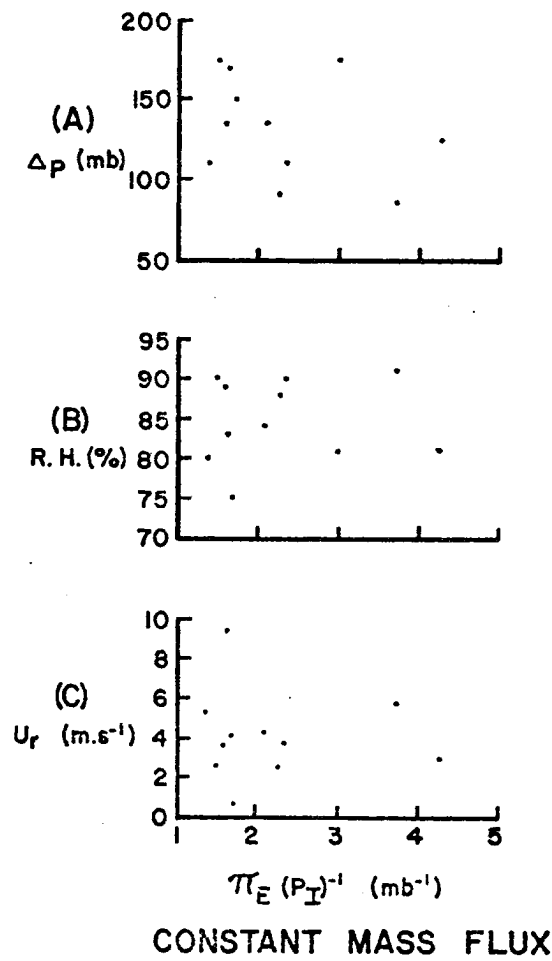


Figure 4.2. A plot of $\pi_E(p_I)^{-1}$ vs. upper layer averaged relative humidity (b,e), depth of the subcloud layer (a,d) and relative inflow of air into the storm (c,f).

It should be pointed out that the specification of π_E provides a relationship between the microphysical parameters but not about their actual value. If the downdraft speed and the rainfall intensity are measured then information about the drop spectrum may be obtained from the definition of π_E .

4.2 Analytical solution of the evaporation equation

The profile of π_E was shown in Section 3.3.1 to be almost constant with pressure in the constant mass flux method. This suggests that we could assume it to be a constant in which case Eq. 3.52 may be easily solved having an analytical solution of the form

$$\Delta\chi = \Delta\chi_I e^{-(p - p_I)/\pi_E} + \frac{d\chi'_w}{dp} \pi_E (1 - e^{-(p - p_I)/\pi_E}). \quad (4.1)$$

With the assumption of constant $\pi_E [= \pi_E(p_I)]$ the final level in the mean soundings is reached with an error of 0.07 g/kg in $\Delta\chi$ which corresponds to an error of less than 1% in the temperature of the lower layer. The point is that even an error of 10% in $\Delta\chi$ produces an error of only 2.5% in the temperature and less than 4% in the relative humidity showing that the results are not very sensitive to errors in the value of $\Delta\chi$.

In the constant divergence case, π_E shows a large variability so that the effect of picking it equal to $\pi_E(p_I)$ implies an error of 0.6 g/kg in $\Delta\chi$ or 10% in the relative humidity. If, instead of picking the constant π_E as $\pi_E(p_I)$, we choose it equal to $\pi_E(p_{LCL})$ or the value of π_E corresponding to cloud base, the error decreases to 0.2 g/kg in $\Delta\chi$ and to 4% in the relative humidity.

Equation 4.1 suggests as well as Fig. 4.1 that if the value of π_E is determined from some sort of closure assumption the thermodynamic characteristics of the subcloud layer are readily obtained. Conversely, the value of the relative humidity in downdraft outflows may provide a way of estimating further the range of variability of π_E .

The value of $\Delta\chi$ may be related to the change of mixing ratio along a wet adiabat $\frac{d\chi'_w}{dp}$ by

$$\Delta\chi = P \frac{d\chi'_w}{dp} \quad (4.2)$$

where P , as may be seen in Fig. 4.3, is the difference between the pressure at the level in question p and the pressure at its lifting condensation level p_{LCL} . Eq. 4.1 may now be rewritten as

$$\Delta\chi = \pi_E \frac{d\chi'_w}{dp} + (P_I - \pi_E) \frac{d\chi'_w}{dp} e^{-(p - p_I)/\pi_E}. \quad (4.3)$$

The second term on the right is smaller than the first one for $P_I - \pi_E < \pi_E$ and decays as p increases so that $\Delta\chi$ will tend asymptotically to the limit

$$\Delta\chi = \pi_E \frac{d\chi'_w}{dp}. \quad (4.4)$$

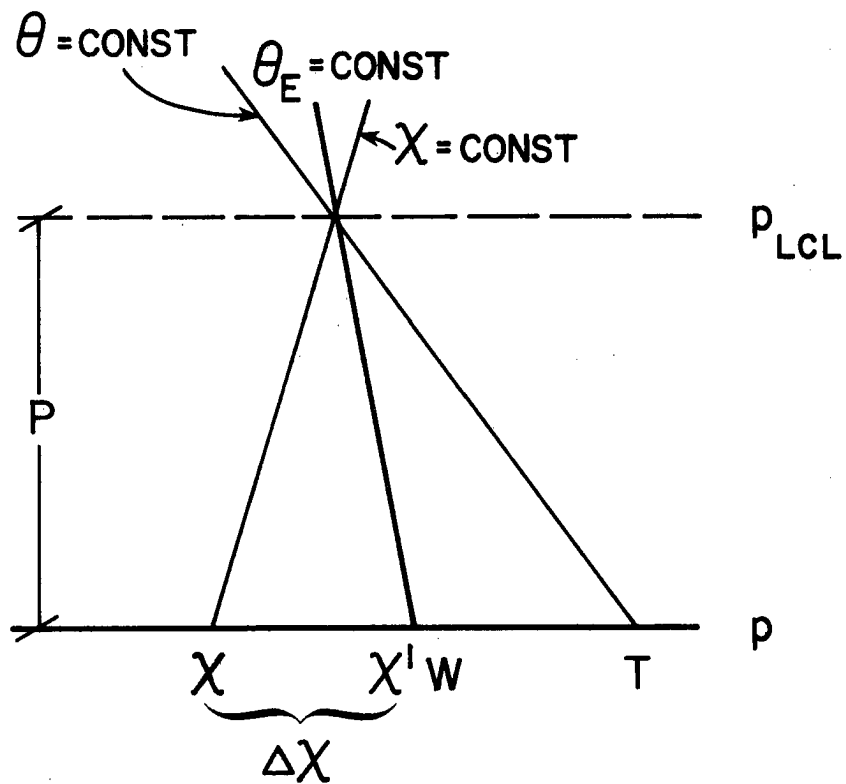


Figure 4.3. The variation of mixing ratio along a constant θ_E line dX'/dp may be approximated, according to the above diagram, by $\Delta X/p$.

Comparing Eq. 4.4 with Eq. 4.2 we see that π_E may be given by P , i.e. by the pressure height to the LCL of the layer. With this physical interpretation for the value of the parameter π_E one may go back to Table 7 and recognize the variation of π_E for the different "after" soundings as a result of the change in P in the subcloud layer. When the first after sounding is taken just after the rain stopped or under drizzle, the value of P is lower than after an hour or so at the time of the launch of the second radiosonde. This is the case for soundings 101-102, 121-123, 122-123, 177-178, 317-318, 325-326. For some cases there is a slight decrease in P with time, the only considerable decrease being in the case of soundings 241-243.

It should be pointed out that the asymptotic behavior of $\Delta\chi$ is reflected in the relative humidity as may be seen in Fig. 4.4 for different values of π_E . The asymptotic value is rapidly attained showing the validity of the reasoning presented above.

The mean value of P was computed for the subcloud layer after the storm passage for all soundings of Table 7 and its value plotted in Fig. 4.5 against π_E . The dashed line indicates $\pi_E = \bar{P}$ as may be seen, it fits the data very well.

The main conclusion of this chapter is that P , in the subcloud layer after the storm passage provides through the definition of π_E in Eq. 3.49 or 3.50, information about the relationship between raindrop spectra and downdraft speeds. The implications of this result are discussed in the following section.

4.3 Suggestions for future research

The use of the parameter π_E in a predictive way will only be possible if some relationship with environmental variables is found.

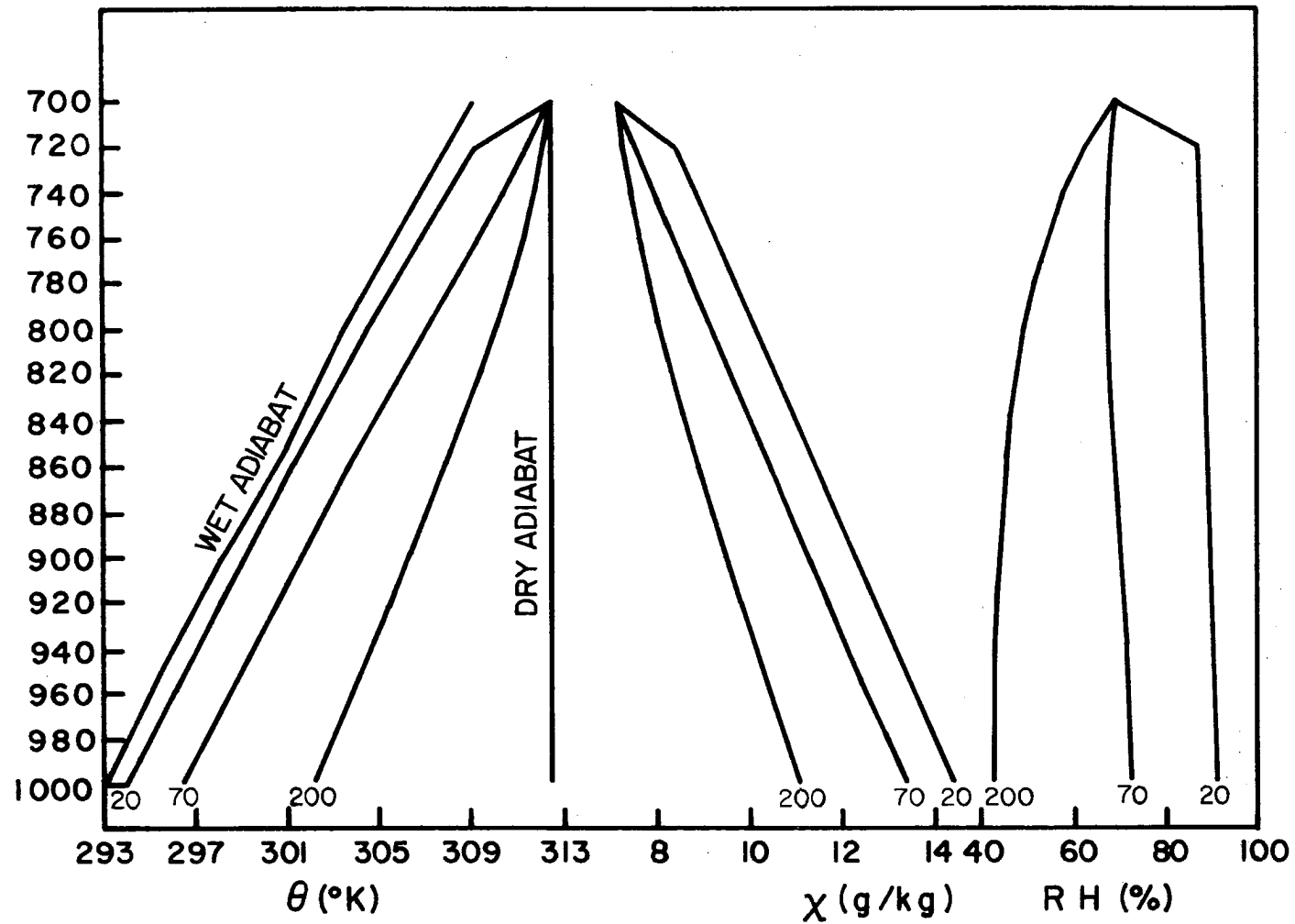


Figure 4.4. Vertical profiles of potential temperature, mixing ratio and relative humidity for different values of π_E (constant mass flux approach) for different starting conditions.

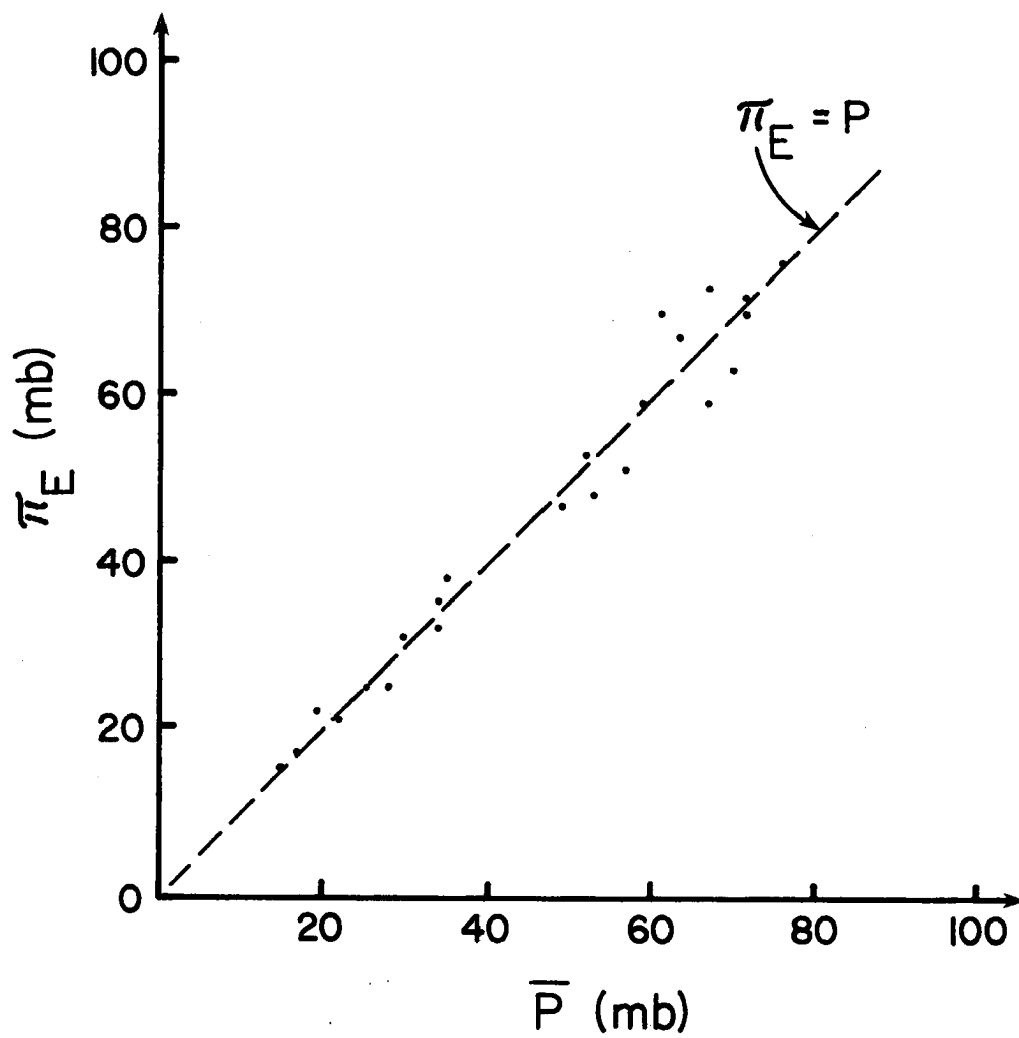


Figure 4.5. A plot of π_E against the mean value of P for the subcloud layer after the storm passage. The dashed line indicates the condition $\pi_E = P$.

Fig. 4.2 did not show any evidence of such a relationship but the small number of data points could explain this lack of dependence. Thus, the most immediate research to be done should be to investigate this topic for different storms and preferably for a considerable number of them. The testing of the validity of the proposed parameterization should be eventually done in the sequence:

- 1) Rawinsonde launched before the storm passage
- 2) Measurement of the drop spectrum and downdraft speed at several levels below 600 mb, inside the storm
- 3) Rawinsonde launched after the storm passage.

Items (1) and (3) are the same as those in VIMHEX-72. The big problem is item (2); the results of Chapter 3 suggest that the downdraft speeds in tropical storms are bounded to be less than 4 or 5 m.s^{-1} so that it should be possible to measure drop-spectra and downdraft speeds with aircraft. Calibrated radar may provide some information on rainfall intensities which contain in itself information of the drop-spectra and of the vertical velocity (Eq. 3.28 and 3.29). By assuming a fixed drop-spectra one may obtain some information of the downdraft speed or vice-versa. Then there is the problem of sampling: what data should be used and what kind of average should be performed? The radar output or the aircraft measurements show conditions over a wide horizontal area some of which is under the influence of the updraft and some under the influence of the downdraft.

The final test would then be done by comparing the value of π_E obtained directly from the observations of drop spectrum and downdraft speed with the value of \bar{P} defined in the previous section, i.e. by the mean value of the pressure height to the LCL in the downdraft outflow.

The model from which π_E has been extracted is a very simple one. It is not certain that the tri-dimensional picture of the actual storm can be satisfactorily squeezed into a single parameter and so this should be further studied!

V. SUMMARY AND CONCLUSIONS

The purpose of this research has been to try to explain the subcloud layer structure after a storm passage by the use of a simple model of evaporation of raindrops in downdrafts that originate in the layer just above cloud base before the storm in accordance to the model proposed by Betts (1976). Two methods have been used one in which the vertical mass flux is constant and another in which it is allowed to vary linearly with pressure, thus allowing a constant divergence. Conditions in rainfall intensities, raindrop radii and downdraft speeds were imposed in order to obtain the desired final thermodynamic structure of the subcloud layer after the storm. A combination of microphysical and thermodynamic variables have been used to define the parameter π_E which may be considered a pressure scale for evaporation $1/\pi_E$ being an evaporation coefficient (similar to an "entrainment" coefficient) for the flux of vapor from evaporating raindrops to the ambient air. Making the assumption of a constant π_E , the relative humidity in the downdraft tends asymptotically to the subcloud layer value after the storm. The parameter π_E may be closely associated with the pressure height to the LCL of the layer.

The constant mass flux approach seems to provide better results than the constant divergence method as has been seen when using a sounding that got into the downdraft air. This may suggest that the divergence in the downdraft air occurs in a very shallow layer close to the surface.

The downdraft speeds obtained diagnostically showed that they should be less than 4 m.s^{-1} , otherwise the rainfall intensities have to

be unrealistically high. This value is reasonable if we consider it as an average through the downdraft in a horizontal scale of several kilometers, thus allowing for peaks of realistic magnitudes.

It has not been possible to find a significant relationship between the parameter π_E and pre-storm variables probably because of insufficient data points. This relationship should be further studied or some kind of closure assumption imposed.

REFERENCES

- Arnason, G., R.S. Greenfield and E.A. Newburg, 1968. A numerical experiment in dry and moist convection including the rain stage. J. Atmos. Sci., 25, 404-415.
- Arakawa, A., and W.H. Schubert, 1974. Interaction of a cumulus cloud ensemble with the large scale environment, Part I. J. Atmos. Sci., 31, 674-701.
- Betts, A.K., 1973. A composite mesoscale cumulonimbus budget. J. Atmos. Sci., 30, 597-610.
- _____, 1976. The thermodynamic transformation of the tropical sub cloud layer by precipitation and downdrafts. J. Atmos. Sci., 33, 1008-1020.
- Berry, E.X., 1968. Modification of the warm rain process. Proc. First Nat. Conf. on Weather Modification, Albany, New York, Am. Meteor. Soc., 81-88.
- Byers, H.R., and R.R. Braham, 1949. The thunderstorm. U.S. Department of Commerce, 287 pp.
- Das, P., 1964. Role of condensed water in the life cycle of a convective cloud. J. Atmos. Sci., 21, 404-418.
- _____, and M.C. Subba Rao, 1972. The unsaturated downdraft. Indian J. Meteor. Geophys., 23, 135-144.
- Donaldson, R.J., Jr., 1961. Radar reflectivity profiles in thunderstorms. J. Meteor., 18, 292-305.
- Frössling, N., 1938. Über die Verdunstung fallender Tropfen. Ger. Beit. Geophys., 52, 170.
- Gray, W.M., 1973. Cumulus convection and large scale circulations: I. BROADSCALE and mesoscale considerations. Mon. Wea. Rev., 101, 839-855.
- Hall, W.D., and H.R. Pruppacher, 1976. The survival of ice particles falling from cirrus clouds in subsaturated air. J. Atmos. Sci., 33, 1995-2006.
- Haman, K.E., and M. Kiewiadoski, 1976. Cold downdrafts in cumulonimbus clouds: a numerical experiment. Proc. of the International Cloud Physics Conference, Boulder, CO., 357-360.
- Hookings, G.A., 1965. Precipitation - maintained downdrafts. J. Appl. Meteor., 4, 190-195.

REFERENCES - Continued

- Johnson, R.H., 1976. The role of convective-scale precipitation downdrafts in cumulus and synoptic-scale interactions. J. Atmos. Sci., 33, 1890-1910.
- Kamburova, P.L., and F.H. Ludlam, 1966. Rainfall evaporation in thunderstorm downdrafts. Quart. J. R. Met. Soc., 92, 510-518.
- Kessler, E., 1969. On the distribution and continuity of water substance in atmospheric circulation. Meteor. Monogr., 10, No. 32, 84 pp.
- Kinzer, G.D., and R. Gunn, 1951. The evaporation, temperature and thermal relaxation - time of freely falling water drops. J. Meteor., 8, 70-83.
- Liu, J.Y., and H.D. Orville, 1969. Numerical modelling of precipitation development and cloud shadows effect on mountain - induced cumuli. J. Atmos. Sci., 26, 1283-1298.
- Ludlam, F.H., 1963. Severe local storms: a review. Meteor. Monogr., 5, pp. 1-30.
- Manton, M.J., and W.R. Cotton, 1977. On the parameterization of rain in cloud models. Submitted to J. Atmos Sci.
- Marshall, J.S., and W. Mck. Palmer, 1948. The distribution of raindrops with size. J. Meteor., 5, 165-166.
- Mason, B.J., 1971. The physics of clouds. 2nd Edition Clarendon Press - Oxford, 671 pp.
- Miller, M.J., and A.K. Betts, 1977. Travelling convective storms over Venezuela. Submitted to Mon. Wea. Rev.
- _____, and R.P. Pearce, 1974. A three-dimensional primitive equation model of cumulonimbus convection. Quart. J.R. Met. Soc., 100, 133-154.
- Moncrieff, M.W., and M.J. Miller, 1976. The dynamics and simulation of tropical squall-lines and cumulonimbus. Quart. J. Roy. Met. Soc., 102, 273-294.
- Ooyama, K., 1971. A theory on parameterization of cumulus convection. J. Meteor. Soc., Japan, 49, Special Issue, 744-756.
- Orville, H.D., and L.J. Sloan, 1970. A numerical simulation of the life history of a rainstorm. J. Atmos. Sci., 27, 1148-1159.
- Ruiz, O., 1975. Mesoscale study of the tropical sub-cloud layer. Atmospheric Science Paper No. 237. Colorado State University, 133 pp.

REFERENCES - Continued

- Seguin, W.R., and M. Garstang, 1976. Some evidence of the effects of convection on the structure of the tropical sub-cloud layer. J. Atmos. Sci., 33, 660-666.
- Squires, P., 1958. Penetrative downdrafts in cumuli. Tellus, 10, 381-385.
- Srivastava, R.C., 1967. A study of the effects of precipitation on cumulus dynamics. J. Atmos. Sci., 24, 36-45.
- Syono, S., and T. Takeda, 1962. On the evaporation of raindrops in a sub cloud layer. J. Met. Soc., Japan, 40, 245-265.
- Takeda, T., 1966. The downdraft in the convective clouds and raindrops: A numerical computation. J. Meteor. Soc., Japan, 44, 1-11.
- _____, 1971. Numerical simulation of a precipitating convective cloud: the formation of a "long lasting" cloud. J. Atmos. Sci., 28, 350-376.
- Wilhemson, R., 1974. The life cycle of a thunderstorm in three dimensions. J. Atmos. Sci., 31, 1629-1651.
- Zipser, E.J., 1969. The role of organized unsaturated convective downdrafts in the structure and decay of an equatorial disturbance. J. Appl. Meteor., 8, 799-814.

BIBLIOGRAPHIC DATA SHEET	1. Report No. CSU ATSP-272	2.	3. Recipient's Accession No.
4. Title and Subtitle Diagnostic analysis of tropical cumulonimbus downdraft structure.		5. Report Date June 1977	
7. Author(s) Maria Faus Silva Dias		8. Performing Organization Rept. No. CSU ATSP-272	
9. Performing Organization Name and Address Department of Atmospheric Science Colorado State University Fort Collins Colorado 80523		10. Project/Task/Work Unit No.	
		11. Contract/Grant No. OCD 74-21678	
12. Sponsoring Organization Name and Address Office for Climate Dynamics National Science Foundation 1800 G Street NW Washington D.C.		13. Type of Report & Period Covered MS Thesis	
		14.	
15. Supplementary Notes			
16. Abstracts <p>The evaporation in the downdraft current associated with tropical cumulonimbus clouds is studied by the use of a simple set of equations for a one dimensional flow. The ideas in Betts' (1976) model are used in the assumption that the air in the sub cloud layer, after the storm passage, originated in a layer of equal depth above cloud base before the storm passage. In this way the layer averaged conditions of temperature and moisture in the sub cloud layer after the storm are obtained from the layer averaged conditions in the upper layer before the storm, using a kinematic-microphysical model in which rainfall intensities downdraft speeds and drop sizes are parameters.</p> <p>It is found that the subsaturation in the downdraft current is specified by a single parameter π_E which may be considered as a pressure scale for evaporation. It is also found that π_E is closely related to parameters derived from the sub cloud layer structure after the storm passage, such as mean relative humidity and mean pressure height to the LCL, providing modellers with a way to check, diagnostically, the range of variation of π_E. It is suggested that π_E should be measured for storms other than the ones used in this study in order to check the validity of the proposed parameterization</p>			
17. Key words, document analysis. Downdraft structure Tropical cumulonimbus VIMHEX			
17b. Identifiers/Open-Ended Terms			
17c. COSATI Field/Group			
18. Availability Statement		19. Security Class (This Report) UNCLASSIFIED	21. No. of Pages 88
		20. Security Class (This Page) UNCLASSIFIED	22. Price